Enhancing bio-oil quality and energy recovery by atmospheric hydrodeoxygenation of wheat straw pyrolysis vapors using Pt and Mo-based catalysts

Eschenbacher, Andreas; Saraeian, Alireza; Shanks, Brent H.; Jensen, Peter Arendt; Li, Chengxin; Duus, Jens Øllgaard; Hansen, Asger Baltzer; Mentzel, Uffe Vie; Henriksen, Ulrik Birk; Ahrenfeldt, Jesper

Total number of authors:
11

Published in:
Sustainable Energy & Fuels

Link to article, DOI:
10.1039/C9SE01254K

Publication date:
2020

Document Version
Peer reviewed version

Enhancing bio-oil quality and energy recovery by atmospheric hydrodeoxygenation of wheat straw pyrolysis vapors using Pt and Mo-based catalysts

Andreas Eschenbacher[a,], *Alireza Saraeian*[b], *Brent H. Shanks*[b], *Peter Arendt Jensen*[a], *Chengxin Li*[c], *Jens Øllgaard Duus*[c], *Asger Baltzer Hansen*[d], *Uffe Vie Mentzel*[d], *Ulrik Birk Henriksen*[a], *Jesper Ahrenfeldt*[a], *Anker Degn Jensen*[a,]*

[a]Department of Chemical and Biochemical Engineering, Technical University of Denmark, 2800 Kgs. Lyngby, Denmark

[b]Department of Chemical and Biological Engineering, Iowa State University, Ames, IA 50011, United States

[c]Department of Chemistry, Technical University of Denmark, 2800 Kgs. Lyngby, Denmark

[d]Haldor Topsøe A/S, 2800 Kgs. Lyngby, Denmark

KEYWORDS. Wheat Straw; Bio-oil; Fast Pyrolysis; Hydrodeoxygenation; TiO_2-supported catalysts; catalysis

ABSTRACT

Atmospheric hydrodeoxygenation (HDO) of wheat straw fast pyrolysis vapors was studied as a promising route for the production of renewable liquid transportation fuels. The performance of TiO_2-supported Pt (0.5 wt.%) and MoO_3 (10 wt.%) catalysts was compared to an industrial Mo-based catalyst using a bench scale reactor operated at atmospheric pressure and up to high biomass-to-catalyst ratios (B:C). Mass and energy balances were complemented by detailed bio-oil characterization including advanced methods such as GC×GC-ToF/MS or−FID and ^{13}C NMR.

At 50 vol.% H_2, all three HDO catalysts effectively reduced the oxygen content of the bio-oils to ~7-12 wt.% (dry basis) compared to a non-catalytic reference (23 wt.% O). MoO_3/TiO_2 was least efficient in conversion of acids (TAN = 28 mg/KOH), while Pt/TiO_2 and MoO_3/Al_2O_3 obtained oils with TAN ~13 mg KOH/g (non-catalytic = 66 mg KOH/g). Compared to the TiO_2-supported catalysts, the industrial Mo/Al_2O_3 catalyst produced higher yields of coke at the expense of condensed bio-oil. MoO_3/TiO_2 performed similar to Pt/TiO_2 in terms of deoxygenation and energy recovery of condensed bio-oil, and by increasing the H_2 concentration to 90 vol.% the energy recovery of bio-oil increased to 39 and 42% at 8 and 10 wt.% O (d.b.), respectively. Pt/TiO_2 showed the highest selectivity to aliphatics and the lowest coke yields, e.g. the coke yield at B:C ~8 was only 0.6 wt.% of fed biomass.

This study demonstrates that by using low-pressures of hydrogen and appropriate HDO catalysts, the quality of bio-oil can be improved without severely compromising its quantity (carbon yield) as observed under catalytic fast pyrolysis conditions.

1 INTRODUCTION

Fast pyrolysis of biomass is a well-developed technology, which can produce bio-oil at yields up to ~60 wt.% (water-free) [1–6]. The integration of biomass-derived pyrolysis oils in existing oil refineries is a potential near-term solution for decreasing our dependence on crude oil and increasing the share of renewables in the transportation sector [7–10]. However, the pyrolysis oil has a high oxygen content of ~35-50 wt.% (present as water and biomass-derived oxygenates), resulting in several adverse properties such as low heating value, high polarity, acidity, and instability upon storage and heating. The fuel properties and miscibility with fossil feedstock can be improved via catalytic deoxygenation of the biomass pyrolysis vapors prior to their condensation [10–19]. Though, these improvements come at the expense of carbon loss as light hydrocarbons, CO, CO_2, and coke [20,21]. Amongst the variety of catalysts tested (without hydrogen addition), microporous HZSM-5 zeolite is considered a suitable solid acid catalyst for production of aromatics and gasoline range products from biomass-derived pyrolysis vapors [22,23]. Nevertheless, rapid deactivation by coking is a major obstacle for their industrial implementation [13,24].

Hydrodeoxygenation (HDO), on the other hand, uses hydrogen to selectively remove oxygen as water without breaking the C-C bonds, and therefore has the potential to obtain higher yields of bio-oil with low oxygen content. Direct catalytic upgrading of biomass pyrolysis vapors by a dual function 5 wt.% Ru/TiO_2 catalyst was reported by Wan et al. [25], who evaluated Ru/TiO_2 in a fixed-bed reactor for upgrading oak and switchgrass pyrolysis vapors at 400 °C and 0.58 bar H_2. Ru/TiO_2 showed a high ketonization activity and light oxygenates were converted to larger, less oxygenated molecules, which improved the stability of the upgraded bio-oil. The TiO_2 support is known to be active for ketonization reactions of acids TiO_2 [26–34] and the defunctionalization of lignin-derived phenolics [35] without the need of hydrogen. As indicated by Wan et al. [25], the

promotion of TiO_2 with a noble metal (Ru) not only adds activity for (hydro-)deoxygenation, but also plays a role in generating oxygen vacancy sites on the TiO_2 surface which promote deoxygenation via an oxygen-vacancy driven reverse Mars−van Krevelen process [36–39]. Using m-cresol as a model compound for Pt supported TiO_2, hydrogen spillover from the metal was proposed to form Lewis-acidic oxygen vacancies on TiO_2, which are capable of aryl-OH bond scission [40]. Over Pt(111), ring hydrogenation to 3-methylcyclohexanone and 3-methylcyclohexanol was found to be the most energetically favorable pathway, while over TiO_2(101), tautomerization and direct deoxygenation to toluene were identified as additional energetically favorable routes. Work conducted at NREL [41] demonstrated the use of 2 wt.% Pt/TiO_2 and 0.5 wt.% Pt/TiO_2 for the continuous upgrading of pine FP vapors at bench-scale. The presence of Pt enhanced the activity and/or prolonged the lifetime of TiO_2 active sites under reducing conditions. It was further proposed that Pt may prolong catalyst lifetime by facilitating the removal of coke precursors from the catalyst surface. The catalytic activity of 2 wt.% Pt/TiO_2 was found to be stable for 13 reaction/regeneration cycles (operated to biomass-to-catalyst (B:C) ratio of ~3), and carbon recoveries of 38 C% with ~16 wt.% oxygen (d.b.) were reported. This level of deoxygenation allowed further processing of the condensed bio-oil by a single stage hydrotreating. However, post-reaction characterization showed an increase in Pt particle size [41], indicating irreversible catalyst deactivation through sintering.

Molybdenum trioxide (MoO_3) was found active for vapor-phase HDO of pyrolysis model compounds and real biomass at low hydrogen pressures [42–45]. It has been reported that MoO_3 undergoes partial carburization during reaction to from oxycarbide- and oxycarbohydride-containing phases. This indicates that surface carbon plays an important role in the activity of MoO_3 under HDO conditions [44]. Studies conducted in the group of Román-Leshkov [43] found

10 wt.% MoO_3 dispersed on ZrO_2 or TiO_2 active and stable for the HDO of m-cresol at 320 °C and low H_2 pressures (≤1 bar). The supported MoO_3 catalysts selectively cleaved C-O bonds without saturating the aromatic ring, thus yielding toluene at moderate to high conversions. It was found that the ZrO_2 or TiO_2 supports stabilized the active Mo species (Mo^{5+}) on the surface. While hydrogen is crucial for retaining HDO activity in bulk MoO_3, it can also change the speciation of active species on the catalyst surface by over-reduction to lower oxidation states with lower reactivity [42,46]. Murugappan et al. [47] tested 10 wt.% MoO_3/TiO_2 and MoO_3/ZrO_2 at 500 °C and H_2 pressures ≤0.75 bar for HDO of pine FP vapors. The supported MoO_3 (10 wt.%) catalysts achieved complete deoxygenation to olefinic and aromatic hydrocarbons at low biomass-to-catalyst (B:C) ratios <0.2. Furans and phenols were found to increase until B:C ~0.6 before slowly declining. For higher B:C ratios, the primary vapors were observed breaking through the catalyst bed. The bare TiO_2 support was reported to show minimal catalytic activity compared to MoO_3/TiO_2 [47]. Others [48] reported a yield of ~43 C% C_4+ hydrocarbons with ~6 wt.% oxygen from upgrading of pine FP vapors in a fluidized bed with an industrial Mo based catalyst.

It is further important to note that the degree of deoxygenation (DOD) of pyrolysis vapors can be enhanced by increasing the H_2 partial pressure [42,48–50]. Higher H_2 pressure can also lead to increased hydrogenation of aromatic rings and olefins to their saturated counterparts. Techno-economic analysis showed that for atmospheric HDO the catalyst cost (e.g. the noble metal loading) and the biomass feedstock price are the primary contributors to the minimum selling price of fuel obtained after hydrotreating [41]. Thus, it is important to consider these factors when designing and testing catalysts for HDO. Since MoO_3 is considerably cheaper than noble metals it might be beneficial to use MoO_3 based catalysts if similar catalytic performance can be achieved.

Catalytic upgrading of fast pyrolysis vapors can be conducted in a one-reactor system, where biomass is fed into a fluidized catalyst bed (*in-situ* configuration [51,52]), or in a two-reactor system in which the catalytic upgrading is performed in a separate reactor downstream of the pyrolysis reactor (*ex-situ* configuration [52,53]). Compared to woody biomass, wheat straw contains a much higher content of alkaline ashes such as K, Ca, Cl and Mg. The direct contact with the catalyst in an *in-situ* upgrading configuration can thus lead to transfer of the alkalines and poisoning of catalytic sites [54–57]. In order to circumvent deposition of biomass indigenous ashes on the catalyst and allow for determination of catalyst coking without the need of char separation, the ex situ configuration was employed in this work.

Based on above research, in this work the deoxygenation performance of a 10 wt.% MoO_3/TiO_2 catalyst, an industrial Mo catalyst similar to that used in ref. [48], and a 0.5 wt.% Pt/TiO_2 catalyst were compared for the deoxygenation of wheat straw pyrolysis vapors in a continuous bench scale unit. Mass and energy balances and a detailed analysis of the bio-oil properties allowed comparing the performance of these HDO catalysts with frequently used solid acid catalysts such as γ-Al_2O_3 and HZSM-5 zeolite. We investigated how the yield and the quality of bio-oil is influenced by the amount of biomass pyrolysis vapors processed over the catalyst. Addressing this aspect will allow determining the frequency of regeneration needed for maintaining a certain bio-oil quality in a scenario of parallel fixed bed reactors [58]. We further studied to what extent the hydrogen concentration influences the yield and quality of the bio-oil. In addition to commonly reported characterization of bio-oils derived from woody biomass using GC-MS, elemental composition, heating value and TAN, we conducted oil characterization by one- and two-dimensional ^{13}C and ^{1}H NMR, GC×GC-ToF/MS or−FID, basic nitrogen determination, and thermogravimetric analysis

in order to fully investigate the chemical composition and fuel properties of the bio-oils derived from wheat straw FP vapors after atmospheric HDO.

2 EXPERIMENTAL SECTION

2.1 Feedstock

Wheat straw pellets were downsized to <1.4 mm using a hammer mill. The proximate and elemental analysis are shown in Table 1. Experimental details on the feedstock characterization can be found in earlier work [13]. Potassium was amongst the highest concentrated ash components with ~1 wt.% (d.b.).

Table 1. Properties of wheat straw feedstock.

Proximate analysis	
Moisture (as received (a.r.)),	8.8 wt.%
Volatiles (dry basis, (d.b.)	66.8 wt.%
Fixed carbon (d.b., by diff.)	18.5 wt.%
Ash (d.b.)	5.9 wt.%
Elemental composition (dry and ash-free basis (daf))	
Nitrogen %	0.8 wt.%
Carbon %	50.4 wt.%
Hydrogen %	5.6 wt.%
Sulfur %	0.1 wt.%
Oxygen % (by diff.)	43.1 wt.%

2.2 Catalyst preparation

In order to achieve a high dispersion of Pt particles, 100 g of Pt/TiO_2 with a target Pt loading of 0.5 wt.% was synthesized via strong electrostatic adsorption following the procedure described by Griffin et al. and references therein [41,59,60]. The pH of an aqueous solution (~500 mL) of 1 g of $Pt(NH_3)_4(NO_3)_2$ was adjusted to 11.5 by adding NH_4OH. Titanium(IV) oxide, (Sigma Aldrich, nanopowder, 21 nm primary particle size (TEM), ≥99.5% trace metals basis) was soaked for 24 h in the solution containing 5.7×10^{-4} M Pt. After impregnation, the catalyst suspension was dried at room temperature for 48 h and then at 60 °C overnight. The catalyst was downsized to 250-850 μm via pelletizing/crushing and filled into the catalytic reactor, where it was calcined/reduced in

147 flowing 5% H_2/N_2 at 450 °C for 5 h. The catalyst was passivated in flowing 1% O_2/N_2 at room
148 temperature before taking a sample for pre-reaction analysis.
149 100 g of 10 wt.% MoO_3/TiO_2 was prepared via wet impregnation: Ammonium molybdate
150 tetrahydrate (Sigma-Aldrich, 99.98% trace metals basis) was dissolved in 80-160 mL nanopure
151 water and added to 10-20 g of TiO_2 (Sigma Aldrich, nanopowder, 21 nm primary particle size
152 (TEM), ≥99.5% trace metals basis). The paste was mixed vigorously overnight using a magnetic
153 stirrer and then dried at 110 °C for 24 h. The dried solid was transferred to a ceramic crucible and
154 calcined at 550 °C (10 °C/min) for 4 h under static air. In addition, 100 g of bare TiO_2 support
155 (same as for preparation of MoO_3/TiO_2 and Pt/TiO_2) was prepared after calcination at the same
156 conditions used for preparation of MoO_3/TiO_2. Prior to reaction tests, all catalysts were reduced
157 for 2 h at 450 °C under reaction atmosphere (50 or 90 vol.% H_2).

158 ## 2.3 Catalyst characterization

159 The Mo loading of the MoO_3/TiO_2 catalyst was determined by X-ray fluorescence (XRF)
160 following the procedure described in earlier work [13]. For the quantification of Ti and Pt in the
161 Pt/TiO_2 catalyst, 0.1-0.15 g finely ground sample was weighed accurately and transferred
162 quantitatively into a Teflon microwave digestion vessel in duplicate. 9 ml of 37% HCl (p.a.
163 quality), 3 ml of 65% HNO_3 (p.a. quality) and 2 ml of 47-51% HF (p.a. quality) were added and
164 the sample was digested at 200 °C for 20 minutes in a Milestone Ethos UP microwave digestion
165 unit yielding a clear sample solution. The sample solution was then transferred to a 100 ml
166 volumetric flask and filled to the mark with pure water (18.2 MΩ). The contents of Ti and Pt in
167 the sample solution were quantified by Inductively Coupled Plasma-Optical Emission
168 Spectrometry (ICP-OES) with an Agilent 720 ES ICP-OES instrument. The sample was analyzed
169 with suitable dilution and the emission signal from several Ti and Pt specific emission lines were

compared to the signal from certified calibration standards containing 0–10 mg/l for Ti and 0–2.5 mg/l for Pt. The precision of the analysis was ±3% relative with 95% confidence.

For analysis of the Pt/TiO_2 catalyst by transmission electron microscopy (TEM), the catalyst was ground in a mortar and sieved to <50 μm before adding them on a copper TEM grid with lacey carbon film. TEM images were acquired using a Tecnai T20 G2 (at an acceleration voltage of 200 kV). For acquisition of X-ray diffraction (XRD) patterns, samples were analyzed in powder form using a zero background holder on a Siemens D500 x-ray diffractometer operated with MDI Datascan software. A copper x-ray tube operating at 45 kV and 30 mA was used in combination with a Ni filter, 0.3 degree divergence and anti-scatter slits, and a 0.15 degree detector slit. A graphite monochromater was tuned to the Cu K-alpha line. Samples were scanned from 10 to 70 degrees two-theta with a step size of 0.05 degrees and a dwell time of 2 seconds per step. The patterns were processed using Jade software version 9.5 from MDI.

N_2 physisorption was carried out on a Quantachrome Novatouch apparatus at liquid nitrogen temperature. Prior to the measurement, the samples were outgassed under vacuum at 350 °C overnight. The specific surface area (S_{BET}) was calculated by the Brunauer-Emmett-Teller (BET) method. The total pore volume (V_{total}) was calculated from the amount of adsorbed nitrogen at the relative pressure of $p/p_0 = 0.99$. The Barrett-Joyner-Halenda (BJH) pore size distribution was derived from the adsorption branch of the N_2 physisorption isotherm.

Temperature programmed desorption (TPD) of ammonia was conducted for the characterization and quantification of the catalyst's acid sites. The measurements were performed using a Micromeritics Autochem II 2920 Chemisorption analyzer. The samples were first heated to 500 °C at 20 °C/min in 20 mL/min He and held for 1 h to remove moisture. Next, the sample temperature was decreased to 450 °C, and the catalyst was reduced in a 10 vol.% H_2/He mixture for 2 h at the

same flowrate. Then, the temperature was lowered to 100 °C and NH_3 was adsorbed for 30 min by flowing 10 vol.% NH_3/He at 20 mL/min. Any weakly adsorbed NH_3 was purged with He for 60 min at 20ml/min. The sample was then heated to 500 °C at 10 °C/min under the same flow conditions and the NH_3 desorption was recorded using a thermal conductivity detector (TCD).

Diffuse reflectance infrared Fourier transform spectroscopy (DRIFT) of pyridine-loaded samples was performed following the procedure reported previously [61] with the modification that the catalyst was reduced at 450 °C for 1 h in a flow of 10 % H_2/N_2 before cooling the sample to 150 °C for acquisition of the spectra of the reduced catalyst. The flow was then changed to argon and pyridine was adsorbed on the reduced catalysts from the vapor phase for 30 min using a bubbler operated at room temperature. After flushing any weakly adsorbed pyridine for 30 min, the spectra of the pyridinated sample was acquired. Absorbance from 4000 to 400 cm^{-1} was collected using 64 scans at a 4 cm^{-1} resolution. A background spectrum was recorded with pure KBr at 150 °C.

2.4 Pyrolysis unit

A detailed description of the bench scale fast pyrolysis unit is found in earlier work [13], and a flow sheet is provided in Fig. S1. In this work, tests were conducted in either 50 vol.% or 90 vol.% hydrogen (balance nitrogen) at a total flowrate of ~8.7 Nl/min and a maximum operating pressure of ~0.1 bar above atmosphere. The biomass feeding-rate on a dry and ash-free basis (daf) was ~3 g/min. The pyrolysis reactor, the cyclones, and the hot gas filter were externally heated to 530 °C, 450 °C, and 350 °C, respectively. In earlier work [62], the experimental uncertainty in terms of ±2 standard deviations for the yields of gas, organic liquid, reaction water, and char was estimated to 2.1 wt.%, 0.4 wt.%, 0.8 wt.% and 3.8 wt.%, respectively. In this work, a catalyst mass of 100 g was used and the typical duration of the assays was ~2 h for tests run to B:C ~4 and ~4 h for tests run to B:C ~8. A catalytic upgrading temperature of 450 °C was found optimal by Wang

et al. [48] for the industrial Mo/Al_2O_3 catalyst, and the same temperature was employed here for the tests with MoO_3/TiO_2. For catalytic upgrading with Pt/TiO_2, the reactor was heated to 400 °C, which has been reported to avoid condensation of the pyrolysis vapors while higher temperatures are undesirable due to a decrease in hydrogen coverage and thermodynamic limitations on ring hydrogenation, which inhibit HDO reaction pathways [41]. Upon contact with the vapors, the temperature of the catalyst (measured in the middle of the fixed bed) increased by ~25-50 °C within the first ~15 min of biomass feeding (B:C ~0.5), after which the bed temperature slowly decreased while remaining 5-25 °C above its set point temperature (see Fig. S2). Condensation was achieved by a three-stage condensation system consisting of i) a condensation stage at 4 °C, ii) an electrostatic precipitator (ESP) for collection of aerosols that were generated during the initial quench, and iii) a condensation stage at -60 °C consisting of a series of impingers immersed in a dry-ice/EtOH bath. The dry gas was analyzed continuously for CO and CO_2 by nondispersive infrared and O_2 by paramagnetism, and every ~10 min a sample was analyzed by GC-FID/TCD for analysis of C_1-C_6 hydrocarbons and H_2.

2.5 Oil characterization

Each experiment yielded five different liquid fractions, which were kept refrigerated at 5 °C in order to minimize ageing reactions. Liquid collected at the 4 °C condensation stage and the -60 °C condensation stage spontaneously phase separated into an aqueous and organic-rich phase, while a single-phase organic-rich oil was collected at the ESP. The three oil fractions and the two aqueous fractions were combined in the proportion of their yields for further analysis. The moisture content and elemental content (CHN, O by difference) of the total bio-oil and aqueous phase was determined by Karl−Fischer titration and elemental analysis according to the details described elsewhere [13]. The higher heating value of the bio-oil (d.b.) was calculated based on the elemental

composition using an empirical formula according to Channiwala and Parikh [63]: $HHV\ [\mathrm{MJ/kg_{d.b.}}] = 0.3491 \times \mathrm{wt.\,\%\ C} + 1.1783 \times \mathrm{wt.\,\%\ H} - 0.1034 \times \mathrm{wt.\,\%\ O} - 0.0151 \times \mathrm{wt.\,\%\ N}$.

The oil and aqueous fractions were analyzed using a GC-MS/FID Shimadzu QP 2010 Ultra apparatus equipped with a Supelco Equity 5 column. Identification and quantification of the species in the samples were performed by the mass spectrometer (MS) and flame ionization detector (FID), respectively. Aqueous samples were analyzed directly while the oil samples were diluted in a 1:9 volumetric ratio in acetone. The initial temperature for the GC column was held at 40 °C for 10 min and the column was heated to 250 °C with an initial heating rate of 2 °C/min to 100 °C followed by an increased heating rate of 8 °C/min. A split ratio of 80 was used at the injection port (280 °C). The MS scanning was set to a range of 20 to 300 m/z. The selectivity of different product groups was calculated based on the FID area percentage after correcting the FID areas taking into account the effective carbon numbers of each compound as outlined by Schofield [64]: $\mathrm{Selectivity}_{\ \mathrm{product\ group}} = \frac{\sum \mathrm{FID\ areas\ of\ compounds\ in\ product\ group}}{\sum \mathrm{FID\ areas\ of\ all\ compounds}} \times 100\%$.

The condensed oil fractions were further analyzed for their total acid number (TAN) following ASTM D664, and for their basic nitrogen content following UOP Method 269-10. Using the methodology reported by Dayton and coworkers [65,66], the evaporation behavior of the oils was studied by thermogravimetric analysis (TGA). About 20 mg of oil was loaded into a Pt crucible with lid shortly before start of the temperature program in order to minimize the loss of volatiles. The temperature was increased at a rate of 10 °C/min to a final temperature of 650 °C in 150 ml/min N_2 flow.

Bio-oil samples obtained in the 50 vol.% H_2 atmosphere without catalyst and at B:C ~4 from atmospheric HDO with the three different catalysts were further characterized by GC×GC-ToF/MS or-FID. In addition, bio-oil obtained from vapor upgrading with MoO_3/TiO_2 at

an increased H_2 partial pressure (90 vol.%) was analyzed. For the analysis, a LECO® Pegasus 4DTM instrument was used that included an Agilent 7890A GC equipped with a Gerstel® CIS 4 PTV inlet, a secondary oven, a quad-jet, dual-stage cryogenic-based (liquid N_2) modulator, a time-of-flight (ToF) mass spectrometer (MS) and a flame ionization detector (FID). The primary (1D) and secondary (2D) columns were Restek® Rtx-1701 and SGE® BPX5, respectively. 0.3 mm^3 sample, diluted 1:1 in THF, was injected in pulsed split mode (split ratio 1:100) into the PVT inlet at 40 °C, and then raised to 300 °C (10 °C/s), with a total hold up time of 1.5 min. The main oven with the 1D column was held at 35 °C for 1.5 min and then ramped to 275 °C at 3 °C/min; the secondary oven and modulator were run with offsets to the main oven of +10 °C and +25 °C, respectively; total run time was 101.5 min. Helium (He) was used as carrier gas at constant flow rate of 1.5 cm^3/min, and the modulation period was 7 sec. The transfer line and ion source of the ToF/MS detector were operated at constant temperatures of 250 °C and 225 °C, respectively. The ToF/MS was run in EI mode at 70 eV and an acquisition rate of 100 spectra/sec for m/z = 41 to 441. The NIST2008 mass spectral database was used as reference. For group quantification, the FID was used. The detector was operated at 300 °C and with a sampling rate of 100 Hz. Based on the GC×GC-ToF/MS analysis the compounds were classified into 13 groups: aliphatics (paraffins/naphthenes), monoaromatics (alkylbenzenes/naphthenobenzenes), di/tri-aromatics, carboxylic acids, pyrroles/nitriles, pentanones/hexanones, furanones/furfuryl alcohols, aliphatic ketone/other aliphatic oxygenates, indanones/benzofurans/dibenzofuranes, phenols/methoxybenzenes, methoxy-phenols, hydroxylated di/tri-aromatics, and dihydroxylated benzenes. The relative amount (FID area-%) of each compound class was estimated as the sum of areas of all detected peaks in that class divided by the total peak area of all compound classes. ChromaTof® 4.72 GC×GC software was applied for data acquisition and exporting of raw data as

CDF files. Successively, pixel-based analysis (proprietary software developed by Copenhagen University) of CDF files was applied for setting up group integration templates and quantification of relative amounts (area-%) of compound classes.

Selected bio-oils were further analyzed by ^{1}H, ^{13}C NMR and 2D HSQC NMR analysis. Details of the used instruments and experimental conditions have been reported earlier [13]. The quantitative ^{13}C integration was performed following the procedure suggested by Ben and Ragauskas [67], while taking into account the modifications suggested by Happs et al. [68]. For ^{1}H NMR, the relative distribution of the different chemical groups was obtained by assigning the functional groups to their chemical shift ranges. The water region (3.6−3.3 ppm) was excluded for this comparison.

3 RESULTS AND DISCUSSION

3.1 Catalyst properties

The catalyst properties are shown in Table 2. The metal loading of the TiO_2-supported Pt and Mo catalysts was determined to be 0.61 wt.% Pt and 5.8 wt.% Mo (theoretical loading of 10 wt.% MoO_3 = 6.7 wt.% Mo). The XRD pattern of the fresh prepared MoO_3/TiO_2 catalyst closely resembles the pattern of the bare TiO_2 support (see Fig. S3), indicating that the MoO_3 is well dispersed on the support. Only few minor additional peaks are observed at 2θ = 23.3°, 33.6°, and 49.2°, which are associated with crystalline MoO_3 clusters [47]. The isotherms and pore size distribution obtained from nitrogen physisorption are shown in Fig. S4 for the Pt/TiO_2 and MoO_3/TiO_2 catalyst. MoO_3/TiO_2 showed a reduced pore volume (0.23 cc/g) compared to Pt/TiO_2 (0.43 cc/g), probably due to the higher loading of the Mo compared to Pt. The pore size distribution by the BJH suggests that MoO_3/TiO_2 has less pores with diameter >400 Å compared to Pt/TiO_2 (see Fig. S4b). Since the crystal size is about 21 nm (210 Å), these larger pores were attributed to voids in between adjacent crystals. The BET surface area of Pt/TiO_2 was 51 m^2/g while that of

MoO_3/TiO_2 was 54 m^2/g. A surface area of 54 m^2/g was also determined by Shetty et al. [43] for a 10 wt.% MoO_3/TiO_2 catalyst . Amongst the tested catalysts, the industrial Mo/Al_2O_3 catalyst had the highest acidity with 0.5 mmol NH_3/g, which is about double the acidity of the Pt/TiO_2 and ~2.5 times the acidity of the MoO_3/TiO_2 catalyst.

The NH_3-TPD in Fig. S5 shows that the reduced Pt/TiO_2 catalyst had both weak acid sites desorbing NH_3 at ~180 °C and medium-strength acid sites desorbing NH_3 at ~300 °C. TiO_2-supported MoO_3 catalyst showed mostly weak acid sites centered at a desorption peak of ~200 °C and to a lesser extent medium strength acid sites, resulting in a lower acidity compared to Pt/TiO_2 (see Table 2).

The catalysts are Lewis acidic as seen by interaction with pyridine at 1612 and 1445 cm^{-1} (see Fig. S6) and the absence of absorbance at 1545 cm^{-1} (pyridine adsorbed on Brønsted acid). At 150 °C MoO_3/TiO_2 showed a higher absorbance of pyridinated Lewis acid sites compared to Pt/TiO_2. Since pyridine is a weaker base than ammonia, it will preferably probe medium- to high-strength acid sites. From NH_3-TPD (Fig. S5) it can be seen that Pt/TiO_2 contains a relative higher fraction of medium-strength acid sites compared to MoO_3/TiO_2. For both samples, the chemisorbed pyridine readily desorbed when heated from 150 °C to 250 °C.

Table 2. Physicochemical properties of TiO_2 supported Pt (0.5 wt.%) and MoO_3 (10 wt.%) catalysts.

	TiO_2	0.5 wt.% Pt/TiO_2	10 wt.% MoO_3/TiO_2	Mo/Al_2O_3
Metal loading	n.d.	0.61	5.8[b)]	n.d.
V_{total} at p/p_0 =0.99 (cc/g)	0.38	0.43	0.23	n.d.
Surface area [m²/g]	47	51	54	n.d.
Acidity[a)] [mmol NH_3/g]	0.16	0.25	0.19	0.50

[a)]The acidity was determined for the reduced catalysts (reduction for 2 h in 10 vol.% H_2); [b)] loading of molybdenum

Representative TEM images of the prepared Pt/TiO_2 catalyst are provided in Fig. S7. The Pt particles were well dispersed on the TiO_2 support with particle diameters between 0.4 and 3.3 nm

and a mean particle diameter of 1.65 (determined for ~110 particles). A Pt particle size distribution between 0-5 nm diameter has also been reported by others for a 2 wt.% Pt/TiO_2 catalyst [69], albeit their work also showed larger particles >5 nm, which may be related to the higher Pt loading.

3.2 Product distribution

The product distribution obtained from atmospheric pressure catalytic HDO in comparison to two non-catalytic reference cases obtained under inert atmosphere (N_2) and 50 vol.% H_2 are shown in Fig. 1. The numeric values are given in Table S1 and Table S2 for tests conducted in 50 and 90 vol.% H_2, respectively. For reference, the product distributions obtained with an empty catalytic reactor and over 100 g TiO_2 at 450 °C under nitrogen atmosphere are given in Table S3, and the properties of the respective bio-oils are given in Table S4. Mass balances between 90-98% were obtained. Upgrading of the vapors over TiO_2 under nitrogen atmosphere at B:C ~4 increased the formation of light gases, reaction water, and coke while decreasing the yield of condensed organics recovered as oil and aqueous phase (see Table S3). Similarly, the yield of light gases and reaction water increased when applying catalytic HDO, which can be attributed to cracking reactions (C_1-C_5 hydrocarbons), and deoxygenation via decarbonylation, decarboxylation, and hydrodeoxygenation. The yields of gas and coke were higher at low B:C ratios, at the expense of liquid-range organics. With continued operation to higher B:C, the yields of gas and coke decreased due to a reduced catalyst activity, and the yield of condensed organics increased. The aqueous phase obtained without catalyst under N_2 atmosphere contained an appreciable amount of organics (~11 wt.% of fed biomass), which decreased to 8 wt.% of fed biomass when the test was performed in 50 vol.% H_2 while obtaining a slightly higher yield of oil phase. This observation is tentatively attributed to a low degree of hydrodeoxygenation of the most reactive vapor compounds via contact of the vapors with i) the metal surface of the pyrolysis reactor/cyclones/catalytic reactor and ii) the vapor contact with biomass indigenous alkalines and metals both during the pyrolysis

356 and upon vapor contact with the char. The slight deoxygenation can lower the polarity of the
357 oxygenates and thus decrease the loss of organics to the aqueous phase.

358 Atmospheric HDO using Pt/TiO_2 decreased the yield of liquid-range organics and increased the
359 yields of light gases, reaction water, and coke. Operation to higher B:C shifted the yields in the
360 direction of the non-catalytic reference and further increased the yield of condensed organics.
361 Remarkably low coke yields resulted for Pt/TiO_2 toward higher B:C, which will be discussed more
362 in section 3.4. Increased H_2 partial pressure led to an enhanced gas production for Pt/TiO_2 and
363 MoO_3/TiO_2, and increased the yield of reaction water for the latter while no marked increase in
364 hydrodeoxygenation was observed for Pt/TiO_2. Mo/Al_2O_3 produced less liquid-range organics and
365 more coke compared to Pt/TiO_2 at B:C ~4. The yield of ethylene and propylene was the highest
366 for Mo/Al_2O_3 (1.5 wt-%) compared to Pt/TiO_2 (0.9 wt-%) and MoO_3/TiO_2 (1.0 wt-%). It is known
367 that for HDO of acetone over MoO_3, the oxygen is removed while making propene [42]. On the
368 other hand, the yield of C_1-C_3 alkanes was slightly higher for Pt/TiO_2, which is attributed to the Pt
369 catalyzed hydrogenation of some of the alkenes and oxygenates [70]. The initial deactivation when
370 using Pt/TiO_2 also corresponded to a decrease in the concentration of C_2–C_5 alkanes and an
371 increase in the C_2–C_5 alkene concentration (see Fig. S8). The loss of hydrogenation activity may
372 be associated with the blocking of metallic Pt sites, and is in line with observations by Griffin et
373 al. [41]. Besides a lower hydrogenation activity of the Mo/Al_2O_3 catalyst compared to Pt/TiO_2, it
374 is expected that the Al_2O_3 supported catalyst has a higher surface area and in combination with its
375 significantly higher acidity (0.5 mmol NH_3/g), catalytic cracking is favored. This can explain the
376 higher coke and lower oil yields observed for the vapor upgrading over Mo/Al_2O_3 compared to the
377 TiO_2-based catalysts. Slightly more reaction water and less CO/CO_2 was formed with Mo/Al_2O_3
378 compared to Pt/TiO_2. In 50 vol.% H_2, MoO_3/TiO_2 produced the lowest gas yields and highest yield

of liquid-range organics at B:C ~4. The yield of coke and reaction water for MoO_3/TiO_2 was in between the values for Pt/TiO_2 and MoO_3/Al_2O_3 (Fig. 1). An increase in H_2 concentration in the gas (from 50 vol.% to 90 vol.%) increased the yield of light gases and reaction water due to increased hydrodeoxygenation and slightly decreased the coke yield (from 1.7 wt.% to 1.6 wt.% of biomass). The yield of organic oil phase was similar for 90 and 50% vol.% H_2, but less organics were recovered in the aqueous stream when using 90 vol.% H_2. This is attributed to a reduced polarity of oxygenates, as will be elaborated in more detail in section 3.3. For MoO_3/TiO_2, the operation to higher biomass-to-catalyst ratio (7.3 vs. 3.6) decreased the yields of gas, reaction water, and coke while the yield of liquid range organics increased. However, this increase was largely due to a higher fraction of organics recovered in the aqueous stream (from 2.2 wt.% to 3.7 wt.% of biomass).

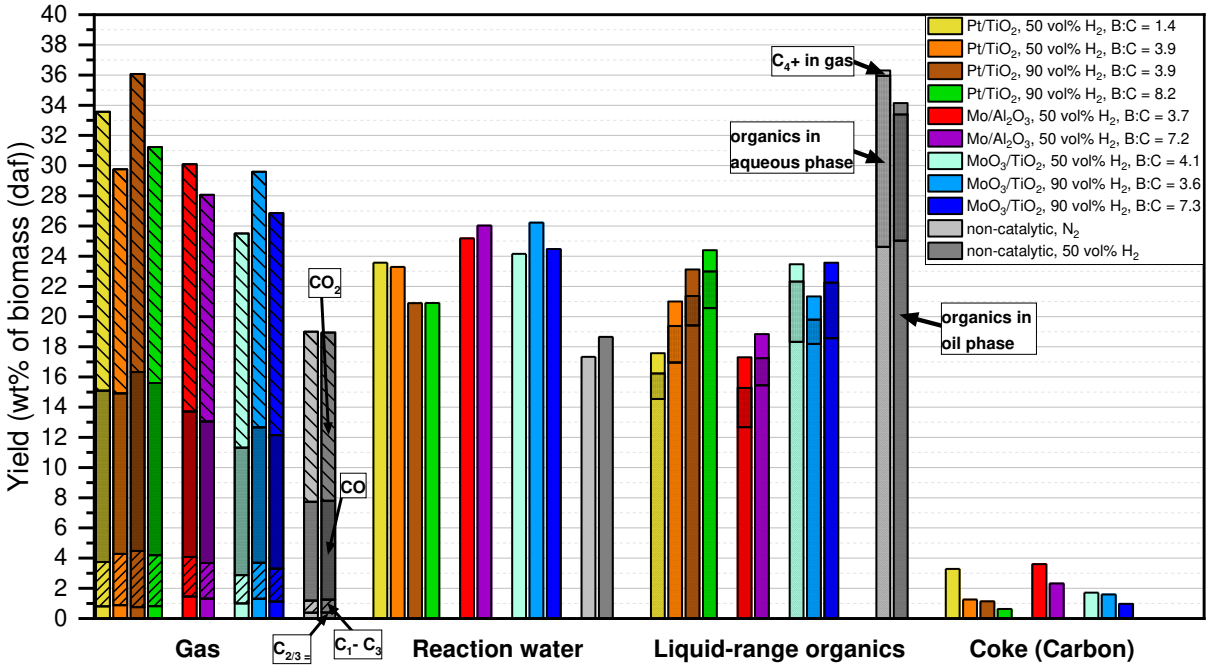

Fig. 1. Product yields based on fed biomass (daf). The char yield was 19.2 ±0.8 wt.%, with the uncertainty being related to the manual collection process.

3.3 Bio-oil properties

Table 3 presents an overview of the bio-oil properties along with the B:C ratio at which the oil was obtained and the experimental conditions such as catalyst temperature and H_2 concentration.

Under N_2 atmosphere, the vapor treatment with bare TiO_2 reduced the oxygen content from ~27 wt.% O (d.b.) to ~20 wt.%, which increased the HHV from ~28 to 31 MJ/kg. The use of TiO_2 under inert atmosphere reduced the total acid number (TAN) of the bio-oil from 71 to 43 mg KOH/g (see Table S4), which is attributed to mild cracking and ketonization reactions [26–32]. The oil obtained without catalyst in 50 vol.% H_2 showed an oxygen content of 23 wt.% O (d.b.). Catalytic HDO in 50 vol.% H_2 to B:C ~4 achieved a clear reduction in the acidity of the bio-oils since the TAN was decreased from 66 mg KOH/g to 12-13 mg KOH/g when using Pt/TiO_2 and Mo/Al_2O_3 while it was decreased to 28 mg KOH/g when using MoO_3/TiO_2. The results indicate that both a high hydrogenation/HDO activity (Pt/TiO_2) and a high acidity (Mo/Al_2O_3) can effectively convert acids, whereas the poorer performance of MoO_3/TiO_2 in TAN-reduction—although still improved compared to the bare TiO_2—likely results from its lower hydrogenation/HDO activity and lower catalyst acidity.

It is known that not only carboxylic acids but also phenolic compounds contribute to TAN, e.g. the acid number for phenol is ~10 mg of KOH/g [15]. The TAN could be further decreased by increasing the H_2 partial pressure, as shown for MoO_3/TiO_2 and Pt/TiO_2, thereby reaching values as low as 2 mg KOH/g at B:C ~4 in the case of Pt/TiO_2, which is the same range as acidic crude oils [71]. At 50 vol.% H_2 and B:C ~4, the MoO_3/TiO_2 catalyst achieved similar deoxygenation compared to Pt/TiO_2 and Mo/Al_2O_3. The moisture content of the bio-oils was reduced from 19 wt.% to 2-7 wt.% after catalytic upgrading. The carbon content of the oils increased from 70 wt.% (empty reactor) to ~77–83 wt.% upon use of catalyst, while the oxygen content was reduced from 23 wt.% to 7-12 wt.%. While complete deoxygenation was not obtained at low B:C ~4, the oxygen

content remained fairly stable and did not significantly increase towards higher B:C, unlike acidic catalysts such as HZSM-5 or γ-Al_2O_3 where usually a rapid deactivation is observed [13,14,62]. A slight deterioration in the oil-properties was observed when comparing the oils obtained at B:C ~4 and B:C ~7 or 8 at the same H_2 concentration, since the TAN and the oxygen content of the oils increased while the revaporization efficiency decreased (**Table 3**). This slight decrease in activity is attributed to the continuous coke build-up rather than a permanent deterioration in the deoxygenation capacity. A stable deoxygenation performance for a TiO_2 supported Pt catalyst during 13 reaction/regeneration cycles was reported by Griffin et al. [41].

The catalytic treatment increased the HHV of the bio-oils from ~28 MJ/kg to ~36-38 MJ/kg. The effective hydrogen index (EHI) as defined by Chen et al. is a calculated indicator of the 'net' H/C ratio of a feed after debiting the feed's hydrogen content for complete conversion of heteroatoms to NH_3, H_2S, and H_2O, according to $EHI = \frac{H-2O-3N-2S}{C}$ [72]. Compounds or mixtures with EHI's <1 led to rapid catalyst coking when upgraded over a ZSM-5 catalyst. Higher EHI's of bio-oils may therefore limit the coking when further processing the bio-oil by fluid catalytic cracking (FCC) units. The atmospheric HDO treatment increased the effective hydrogen index (EHI) from ~0.3 to ~1.0 (**Table 3**). The increase in H_2 concentration from 50 to 90 vol.% increased the EHI of the oils obtained using MoO_3/TiO_2 from 0.95 to 1.09, while the EHI of the oils obtained by vapor treatment with Pt/TiO_2 remained in the range of 1.05. The trend in EHI correlates with the trends in molar H/C ratio, as both parameters are indicative of the hydrogen incorporation, e.g., via hydrogenation of olefins and aromatic rings.

The basic nitrogen content of bio-oils is an important parameter for the processing of the upgraded bio-oils in a FCC unit of a conventional refinery since basic nitrogen compounds (reversibly) poison the FCC catalysts via rapid coking and the combustion of nitrogen containing

440 coke species requires nitrous oxide abatement. The vapor treatment with the HDO catalyst did not
441 markedly affect the basic nitrogen content of the bio-oils compared to the non-catalytic reference
442 (0.4 mass%), and it is known that basic heterocyclic compounds, e.g. pyridines and quinolones are
443 among the most difficult to remove via hydrodenitrification [73]. While some denitrification may
444 have been achieved, the decrease in oil yield (especially at lower B:C) may have led to a
445 concentration of more recalcitrant basic nitrogen species.
446 The volatility and stability of the oils obtained from atmospheric HDO improved significantly
447 upon catalytic treatment, as seen from the weight loss curves during heating of the oils in a TGA
448 (see Fig. S9–S11), The revaporization efficiency [65,66] stated in **Table 3** indicates what fraction
449 of the (water-free) oil had volatized at 350 °C. The revaporization efficiency increased from ~70%
450 to 86–96% by applying atmospheric vapor HDO. Oils obtained using Pt/TiO_2 for vapor HDO
451 showed the highest revaporization efficiency (~95%). At B:C ~4 and 50 vol.% H_2, amongst the
452 three HDO catalysts the revaporization efficiency of bio-oil obtained using the MoO_3/TiO_2 catalyst
453 was the lowest (86%). However, the revaporization efficiency of bio-oils obtained from vapor
454 upgrading with MoO_3/TiO_2 catalysts improved when increasing the hydrogen concentration to
455 90 vol.% H_2. As such, the reduced reactivity and charring tendency of the oils correlates with
456 increased EHI and H/C ratios, which is reasonable since alkanes have a higher volatility and are
457 less reactive compared to (unsaturated) oxygenated compounds.
458

Table 3. Properties of phase-separated bio-oil fraction for catalysts (100 g) and reaction conditions as indicated

Catalyst	-	Pt/TiO_2				Mo/Al_2O_3		MoO_3/TiO_2		
Reactor temperature	500 °C	400 °C				450 °C		450 °C		
H_2 vol.%	50	50	50	90	90	50	50	50	90	90
B:C	-	1.4	3.9	3.9	8.2	3.7	7.2	4.1	3.6	7.3
Yield of oil phase [wt-% (daf)]	25.0	15.8	17.0	19.4	20.6	12.7	17.3	18.3	18.2	18.6
Energy recovery oil + C_4+	37.2	31.5	36.1	41.6	42.3	28.9	32.4	36.6	39.1	38.1
H_2O content [%]	18.7	7.0	2.7	2.6	5.0	1.8	2.8	4.6	2.8	4.3
wt-% N (d.b.)	1.1	1.7	2.3	2.9	2.0	2.8	2.8	2.9	2.7	2.4
wt-% C (d.b.)	70.3	83.0	78.0	78.6	78.2	78.5	77.2	78.2	80.4	78.8
wt-% H (d.b.)	5.2	8.2	8.8	8.7	8.8	8.7	8.5	8.2	8.9	8.5
wt-% O (d.b.)	23.4	7.0	10.9	9.8	11.0	9.9	11.5	10.7	8.0	10.3
Higher heating value (HHV) [MJ/kg]	28.2	37.9	36.4	36.7	36.5	36.6	35.8	35.8	37.7	36.5
Effective hydrogen index	0.34	1.00	1.05	1.04	1.07	1.04	1.00	0.95	1.09	1.02
H/C	0.88	1.18	1.34	1.32	1.34	1.32	1.31	1.25	1.32	1.29
O/C	0.25	0.06	0.11	0.09	0.11	0.09	0.11	0.10	0.07	0.10
TAN [mg KOH/g]	66	13	12	2	12	13	19	28	13	20
Basic nitrogen (mass-%)	0.40	0.52	0.39	0.49	0.38	0.37	0.34	0.37	0.36	0.38
revaporization efficiency @350 °C (% d.b.)	70	95	96	96	95	94	91	86	92	90

The relative abundance of the main compound groups detected by GC-MS/FID in the phase separated aqueous fractions is shown in Fig. 2a. After atmospheric HDO, the aqueous phase organics that could be detected by GC-FID were mainly comprised of phenolics, acids, ketones, and alcohols (see Fig. 2a). The aqueous phase from the non-catalytic reference contained less phenolics and more ester, methoxy-phenol, and (anhydro-)sugar-type compounds. Fig. 2c shows the semi-quantitative yields by multiplying the yield of total organics (d.b.) in the aqueous phase with the selectivity of identified compounds. The atmospheric HDO clearly reduced the yield of acids recovered in the aqueous phase. The yield of acids contained in the aqueous phase increased

471 towards higher B:C, and at similar B:C it decreased when increasing the H_2 concentration. These
472 trends correlate with the TAN of the phase-separated bio-oil fraction (see **Table 3**), and the same
473 observations have been reported for the upgrading of wheat straw FP vapors with solid acid
474 catalysts in N_2 atmosphere [14]. Since acids are difficult to hydrogenate they are likely
475 decarbonylated or converted via ketonization, which can explain a high yield of 2-butanone
476 (ketonization product of acetic acid and propionic acid) and 2-pentanone (ketonization of two
477 propionic acid molecules) observed in the oil phase (see Fig. 3).

478 The selectivity and yields of compounds in the oil phase as detected by GC-MS/FID is shown
479 in Fig. 2c+d. Compared with the non-catalytic reference, the oils obtained from atmospheric HDO
480 contained higher concentrations of hydrocarbons such as aliphatics and monoaromatics, and higher
481 concentrations of phenolics while methoxy-phenols and acids were effectively reduced or even
482 converted completely. Note that the ketonization of acetic acid over TiO_2 would yield acetone
483 [74], which was used as solvent and therefore excluded in the analysis of the oil-phase. The acetone
484 formed from ketonization of acetic acid was likely to some extent converted to propane/propene,
485 in agreement with increased yields of propane/propene compared to the non-catalytic reference.
486 The increase in H_2 partial pressure from 50 to 90 vol.% increased the yield of hydrocarbons, and
487 Pt/TiO_2 was more selective to aliphatics while MoO_3/TiO_2 did not favor ring hydrogenation and
488 favored monoaromatics. The chromatograms of the non-catalytic reference oil (50 vol.% H_2) and
489 two oils obtained after HDO with Pt/TiO_2 and MoO_3/TiO_2 catalysts at B:C ~4 (90 vol.% H_2) are
490 shown in Fig. 3. Interestingly, the alkanes obtained with Pt/TiO_2 at 90 vol.% comprised long chain
491 alkanes such pentadecane, heptadecane, and eicosane, which indicates the occurrence of C–C
492 coupling reactions, possibly via ketonization and subsequent alkylation or aldol condensation with
493 other light oxygenates [25]. The highest yield of aliphatics was 1.7 wt.% of fed biomass. Griffin

et al. [41] found that the concentration of unreacted oxygenates such as acetic acid and methoxyphenols from upgrading pine pyrolysis vapors over 2 wt.% Pt/TiO_2 increased steadily during the course of the reaction to B:C ~3. The analysis of their condensed oil by GC-MS showed a high concentration of phenols and ketones, which agrees with this work; however, a higher concentration of methoxyphenols was reported in Griffin et al.'s work [41]. This is likely related to the higher lignin content of pine compared to wheat straw and the higher oxygen content of the upgraded bio-oil (~16 wt.%, d.b.) reported by Griffin et al. [41] compared to this work (7-11 wt.% O, d.b). In agreement with our observations (Fig. 3), Wan et al. [25] reported significant decrease in acetic acid, hydroxyacetone, methoxy-phenols and dihydrobenzofuran when upgrading fast pyrolysis vapors from oak and switchgrass with 5 wt.% Ru/TiO_2 at 400 °C (0.6 bar H_2), while an increase in acetone, 2-butanone, 2-cyclopenten-1-one, and phenol was observed. The effective conversion of methoxyphenols from wheat straw fast pyrolysis vapors by HDO using the industrial Mo/Al_2O_3 agrees with Wang et al.'s [48] results for upgrading pine fast pyrolysis vapors (*in-situ* reactor configuration). Based on the high selectivity to phenols (Fig. 2c) after atmospheric HDO, phenols are likely an important contributor to the TAN of the upgraded bio-oils [15]. Since the breakage of phenolic C–O bonds requires a high bond dissociation energy of 468 kJ/mol [75], we hypothesize that only the increased hydrodeoxygenation activity at increased H_2 partial pressure allowed to further decrease the yield of phenolics and therefore reduced the TAN of the bio-oils (see **Table 3**).

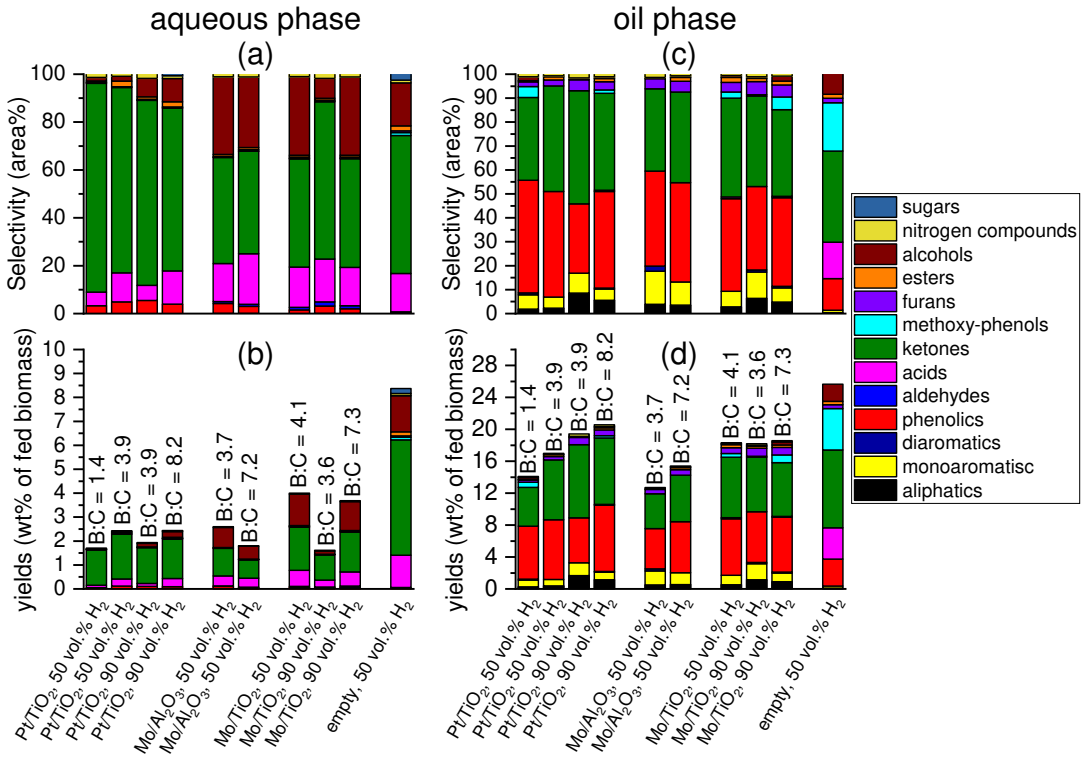

513

514 **Fig. 2.** GC-MS/FID results: (a) Selectivity of compounds (grouped) in aqueous phase. (b) Semi-quantitative
515 yields of compounds in aqueous phase. (c) Selectivity of compounds (grouped) in oil phase. (d) Semi-
516 quantitative yields of compounds in oil phase.

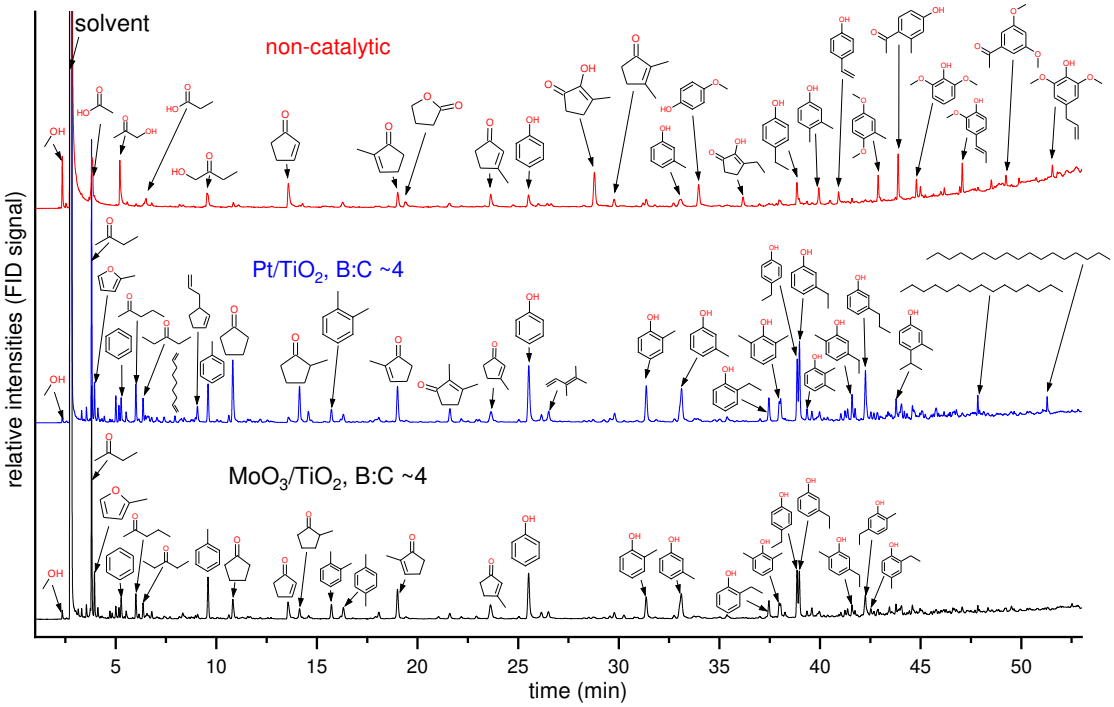

Fig. 3. GC-FID chromatograms of non-catalytic reference (50 vol.% H_2) and two oils obtained after HDO with Pt/TiO_2 and MoO_3/TiO_2 catalyst at B:C ~4 (90 vol.% H_2).

Two-dimensional GC×GC analysis allows characterizing the bio-oil comprehensively based on the spatial separation of polar and nonpolar compounds, thereby expanding the range of volatile compounds that can be analyzed. The 2D GC×GC plots for the non-catalytic oil and oils obtained at B:C ~4 and 50 vol.% H_2 using the three different catalysts are shown in Fig. S12-S16. In addition, the oil obtained from vapor upgrading with MoO_3/TiO_2 at B:C ~4 and 90 vol.% H_2 was analyzed to demonstrate the effect of H_2 partial pressure on the oil composition. The integration results of the different regions in the two-dimensional plots are summarized in Fig. 4. Note that the contribution of acids (Ac), nitrogen containing groups (Nit), and furanones/furfuryl alcohols (Fur) was multiplied by 10 for better visibility. Most noticeably, the GC×GC analysis shows a severe reduction in the yield of Ac, Nit, pentanones/hexanones, Fur, dihydroxylated benzenes, and methoxy-phenols after vapor HDO compared to the non-catalytic reference, in general agreement with the decrease in oxygen content and TAN. On the other the hand, the yield of oxygen-free

hydrocarbons, especially aromatics increased after HDO. The contribution of acids, ketones (Ket), furans, phenols (Ph), and methoxy-phenols (MeO-Ph) was lowest for the industrial Mo catalyst, while this catalyst showed the highest aromatics content. This observation agrees with both the GC-MS/FID results (Fig. 2) and the NMR characterization of the bio-oils (Table 4 and Table 5). The Pt/TiO_2 catalyst was most selective to phenolics, in agreement with the trends suggested by GC-MS/FID (Fig. 2). An increase in the H_2 concentration from 50 to 90 vol.% led to a clear improvement in the bio-oil properties as shown for MoO_3/TiO_2. The selectivity to oxygen-free hydrocarbons (Ali + Ar) increased at the expense of oxygen-containing compound groups. This observation agrees with the findings by GC-MS/FID (Fig. 2) and a reduction in oxygen content and TAN (see **Table 3**).

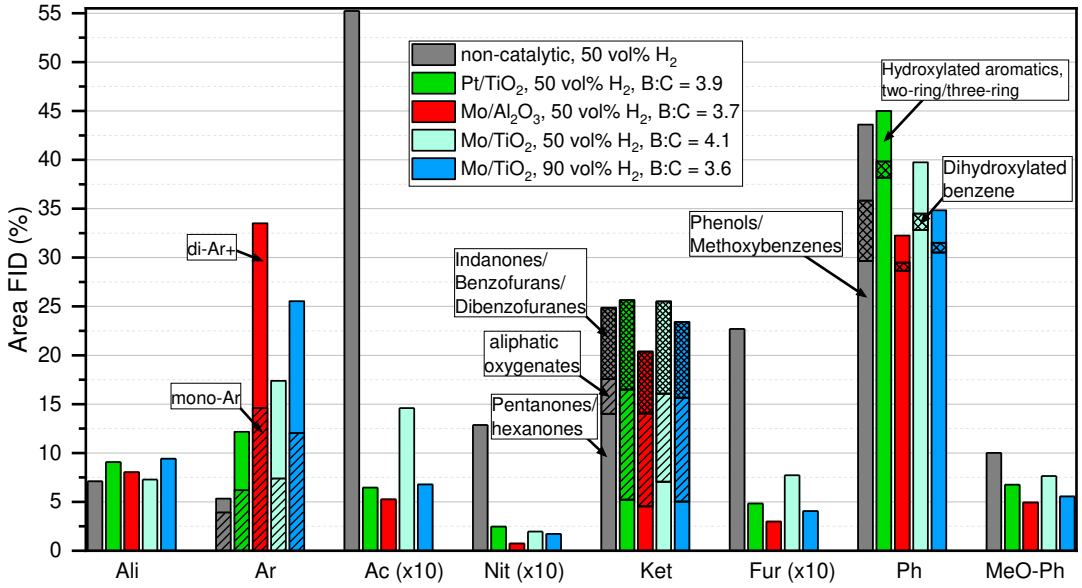

Fig. 4. GC×GC-FID analysis of the bio-oils. The components in the condensed organics are divided into aliphatics (Ali), aromatics (mono and di+ Ar), acids (Ac), pyrroles/nitriles (Nit), ketones (Ket), furanones/furfuryl alcohols (fur), phenols (Ph), and methoxy-phenols. The relative FID area contribution of Ac, Nit and Fur was multiplied by 10 for better visibility.

While gas chromatography methods provide single-compound information, only the fraction volatilizing during injection (~280 °C) is analyzed. Compounds with higher boiling point, light compounds overlapping with the solvent (acetone), or reactive compounds that oligomerize or

form char during the injection are not analyzed. The heating of the oils in the TGA (Fig. S9–S11) indicates that only 56 wt.% of the organics (water-free) volatilized at the injection temperature for the non-catalytic reference oil, while ~83–86 wt.%, 82–85 wt.%, and ~74–83 wt.% of the upgraded oils volatilized when using Pt/TiO_2 , Mo/Al_2O_3, and MoO_3/TiO_2, respectively.

In order to obtain information on the whole composition of the bio-oils, the non-catalytic bio-oil and the bio-oils obtained from atmospheric HDO with the three different catalysts at B:C ~4 in 50 vol.% were analyzed by ^{13}C and ^{1}H NMR. The spectra are provided in Fig. S17-S18 while Table 4 and Table 5 summarize the contribution of different product groups according to their chemical shift range. The atmospheric HDO reduced the contribution of carbonyls from ~15% to ~8-10% and the contribution of aromatic C–O was reduced from ~13 to 7-9% (Table 4). The HDO resulted in a clear decrease of aliphatic C–O groups from ~10 to ~2%, and methoxyl groups were practically removed completely (detection level). While the aromatic C-C and C-H regions overlap to some extent, the sum of aromatic C–C and C–H contributions clearly increased by the catalytic treatment from ~26% to ~32-33% using Pt/TiO_2 or MoO_3/TiO_2 while it increased to 38% using Mo/Al_2O_3.The aliphatic C–H contribution on the other hand was most enhanced for Pt/TiO_2 (48%), followed by MoO_3/TiO_2 (45%) and Mo/Al_2O_3 (42%). While oxygen containing groups were clearly reduced with all three catalysts, under 50 vol.% H_2 the reduction in oxygen containing groups was least pronounced using MoO_3/TiO_2, in agreement with higher TAN and charring propensity of this oil (Table 3). It is worth mentioning that a similar oil quality could be obtained when operating to higher B:C (7.3) at increased H_2 concentration of 90 vol.% (see Table S5). The operating at increased H_2 concentration can thus reduce the frequency of catalyst regeneration in a scenario of parallel fixed bed reactors while maintaining a certain oil quality.

572 The results from ^{1}H NMR analysis (Table 5) show a slightly higher content of aromatic and
573 conjugated alkene hydrogen (8.2−6.0 ppm) after HDO for all catalysts. Aliphatic H connected to
574 oxygen in sugars and related groups (chemical shifts from 3.0- 6 ppm) show a strong decrease
575 from ~14% to ~1-3% after HDO. The oil obtained by HDO with the Mo/Al_2O_3 catalyst showed
576 the highest contribution of aromatics and conjugated alkene H, followed by MoO_3/TiO_2 and
577 Pt/TiO_2, while the aliphatic H was favored in reverse order, in agreement with the ^{13}C NMR results.
578 The increased aliphatic H of the Pt/TiO_2 oil agrees with the increased hydrogen incorporation
579 indicated by the higher EHI and H/C ratios of the Pt/TiO_2-derived oils (see Table 3).

580 The lack of ring hydrogenation was checked for monoaromatics and phenol in excess H_2
581 (99 vol.%) by thermodynamic calculations for temperatures 400–475 °C and hydrogen pressure
582 1–50 bar (see Fig. S24–25). The equilibrium calculations show that higher pressures and/or lower
583 temperatures are needed to hydrogenate the rings.

584 **Table 4**. Carbon percentage based on the ^{13}C NMR analysis of bio-oils obtained in 50 vol.% H_2 atmosphere
585 (atm. pressure) and B:C ~4 for the three different HDO catalysts.

	No catalyst	Pt/TiO_2	MoO_3/Al_2O_3	MoO_3/TiO_2
Carbonyl (215–166.5 ppm)	15.4%	9.8%	8.3%	9.3%
Aromatic C–O (166.5–142 ppm)	12.5%	6.7%	8.6%	10.3%
Aromatic C–C (142–132/125 ppm)[a]	9.2%	4.7%	6.4%	5.4%
Aromatic C–H (132/125–95.8 ppm)[a]	16.5%	28.0	31.8%	26.4%
Aliphatic C–O (95.8–60.8 ppm)	9.9%	2.1%	2.0%	2.4%
Methoxyl (60.8–55.2)	4.2%	0.3%	0.4%	1.3%
Aliphatic C–H (55.2–0 ppm, with exclusion of solvent)	32.4%	48.4%	42.5%	44.8%

586 [a]For catalytically treated pyrolysis bio-oils, the border between aromatic C–C and aromatic C–H was
587 moved downfield from 125 ppm to 132 ppm following the recommendation of Happs et al. [68].

588

589 **Table 5.** Hydrogen percentage based on the ^{1}H NMR analysis of bio-oils, obtained in 50 vol.% H_2
590 atmosphere (atm. pressure) and B:C ~4 for the three different HDO catalysts.

assignment	No catalyst	Pt/TiO_2	MoO_3/Al_2O_3	MoO_3/TiO_2
-COOH (12.5–11.0 ppm)	0.1%	0.1%	0.1%	0.0%
-CHO, ArOH (11.0–8.2 ppm)	0.8%	0.5%	1.1%	0.7%
aromatics and conjugated alkene H (8.2–6.0 ppm)	18.5%	20.6%	23.2%	21.5%
aliphatic OH, -CH=CH-, Ar−CH_2-O−R (6.0–4.2 ppm)	5.6%	1.4%	1.7%	2.7%
R−CH_2−O-R, CH_3−O−R (4.2 –3.0 ppm)	13.9%	0.8%	1.3%	3.6%
-CH_2CH=O, aliphatic H (3.0–2.0 ppm)	24.6%	44.2%	42.8%	40.7%
aliphatic proton (2.0–0 ppm)	36.5%	32.5%	29.7%	30.8%

591 Compared to 1D NMR spectra required for quantification, 2D NMR spectra lower the likelihood
592 of overlapping signals because the signals are spread out into two dimensions. The heteronuclear
593 single-quantum correlation spectroscopy (HSQC) correlates chemical shifts of carbons and
594 protons in a phase sensitive way. The 2D HSQC spectra of oils analyzed by 1D NMR are provided
595 in Fig. S19-S23. Oils obtained from the catalytic vapor treatment with HDO catalysts showed a
596 clear decrease in the contribution of -CH-O- and -O-CH-O- groups, which are mainly present in
597 sugars. Aldehydes were converted almost completely using Pt/TiO_2 while a higher concentration
598 of aldehydes remained for the oil obtained from HDO with Mo/Al_2O_3.

599 3.4 Coke on catalyst

600 The regeneration of coke species on the three HDO catalysts occurred at lower combustion
601 temperatures compared to regeneration of coked Al_2O_3 or HZSM-5 (see Fig. 5a). The TiO_2-
602 supported catalysts showed the lowest combustion temperature. The observation might be a
603 combined effect of a combustion-catalytic effect by Pt and MoO_3, as well as differences in the
604 coke properties. While not further investigated in this work, the coke species from HDO may
605 contain higher H/C ratios compared to the more graphitic coke inside zeolitic micropores. For
606 HDO of a lignin model compound (m-cresol), Shetty et al. [43] reported that an Al_2O_3-supported
607 MoO_3 showed a higher tendency to form refractory graphitic coke compared to TiO_2 and ZrO_2-
608 supported MoO_3 catalysts, thereby requiring higher temperatures for oxidative regeneration, which
609 agrees with our observations. The onset of coke-combustion for the coke deposited on TiO_2 from

610 upgrading under N_2 atmosphere occurred at higher temperatures (~275 °C) compared to the Pt and
611 MoO_3-promoted TiO_2 catalysts (not shown). Fig. 5b shows a comparison of the deposited mass of
612 coke (carbon) per mass of coke-free catalyst towards higher B:C ratios for the different HDO
613 catalysts and acidic catalysts such as γ-Al_2O_3 and HZSM-5 zeolite [14]. The coking propensity of
614 γ-Al_2O_3 is rather high, while the microporosity of HZSM-5 limits the coke formation [14]. The
615 coking propensity of bare TiO_2 under nitrogen atmosphere was in the same range as HZSM-5. The
616 Pt/TiO_2 catalyst formed less coke per mass of catalyst compared to HZSM-5 zeolite and the bare
617 TiO_2 support, which could indicate that hydrogenation of coke precursors and coke scavenging
618 occurred near the active Pt sites. Coke scavenging was observed in micropyrolyzer tests where H_2
619 continued to flow over the catalyst in between pyrolysis vapor pulses [47]. Remarkably, the HDO
620 using Pt/TiO_2 resulted in only a slight additional buildup of coke compared to the coke that had
621 initially deposited at B:C ~1.2, even though the catalyst was still active and improved the fuel
622 properties of the condensed bio-oil up to high B:C of ~8 (see Table 3). This is attractive as it limits
623 carbon losses to coke and eventually CO_2 during the catalyst regeneration. The coking propensity
624 of MoO_3/TiO_2 was slightly higher compared to Pt/TiO_2, yet below the coking propensity of
625 HZSM-5. We further note that an increase in H_2 concentration from 50 to 90 vol.% led to a slight
626 decrease in coke deposition for the MoO_3/TiO_2 and Pt/TiO_2 catalysts (Fig. 5). Compared per
627 surface area of catalyst, 0.96 and 1.29 mg C/m^2 deposited using Pt/TiO_2 and MoO_3/TiO_2 catalyst
628 at 50 vol.% H_2, which decreased to 0.86 and 1.07 mg/m^2 at increased H_2 concentration of 90 vol.%.
629 Amongst the three tested HDO catalysts, the coking propensity of the industrial MoO_3/Al_2O_3 was
630 the highest, which we tentatively attribute to a higher surface area and acidity of the Al_2O_3 support
631 compared to TiO_2.

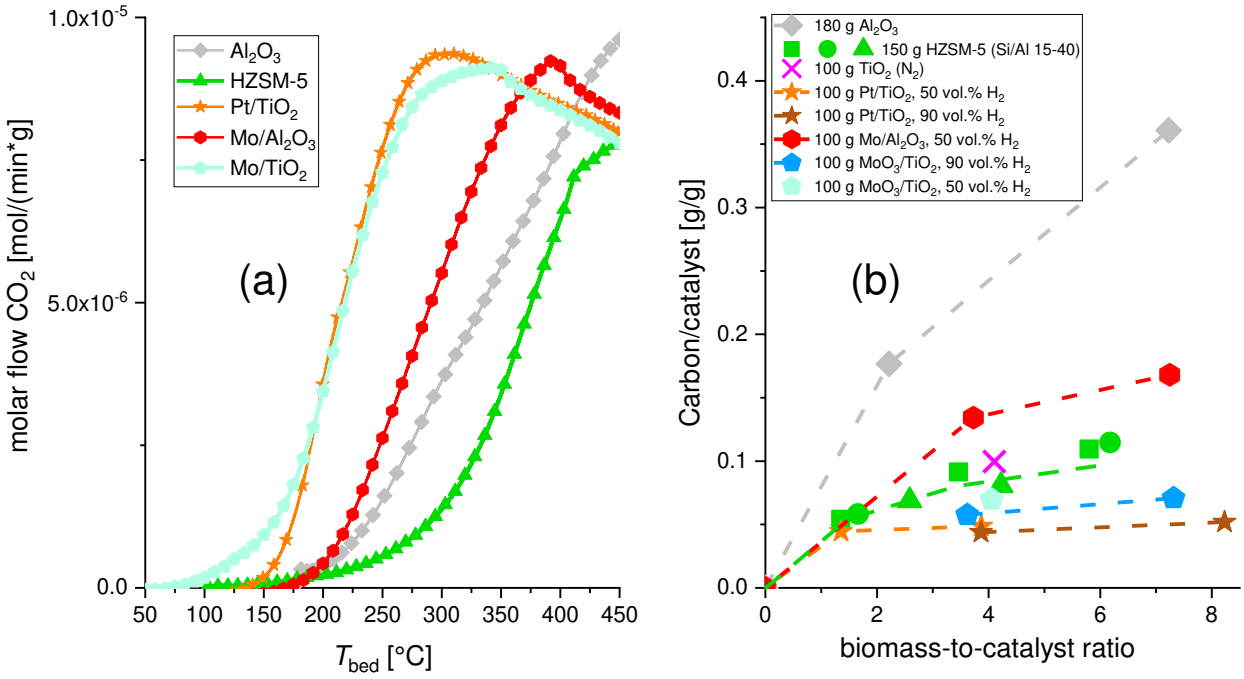

Fig. 5. (a) CO_2 evolution during coke combustion (B:C ~4) of the full catalyst bed in ~2 vol.% O_2/N_2 during heating at 1 °C/min. HDO tests were conducted in 50 vol.% H_2. (b) Deposited mass of carbon in coke per coke-free catalyst for different catalysts and towards higher B:C ratios. Data points for γ-Al_2O_3 and HZSM-5 have been reported earlier [14,62].

3.5 Catalyst stability

In order to investigate potential sintering of small Pt particles, the Pt/TiO_2 catalyst was re-analyzed by TEM after four cycles of reaction and regeneration. Representative TEM images and the particle size distributions obtained from ~200 particles of ~10 different sample locations are shown in Fig. S26. The Pt particles remain well dispersed on the support. While the peak of the particle size distribution remains centered at ~1.5 nm similar to the pre-reaction characterization (Fig. S7c), the post-reaction particle size distribution extended to larger particles up to ~5 nm (Fig. S26f). The post-reaction characterization of the regenerated TiO_2-supported catalysts showed only minimal changes in surface area, as the surface area slightly increased from 51 to 54 m^2/g for Pt/TiO_2 and slightly decreased from 54 to 49 m^2/g for MoO_3/TiO_2. Griffin et al. [41] reported minimal changes to the TiO_2 support after 13 reaction/regeneration cycles, albeit a more

pronounced increase in Pt particle size was observed in their work—yet without any apparent impact on performance.

A sample of spent MoO_3/TiO_2 catalyst that was obtained after three reaction-regeneration cycles using straw as feedstock and after three additional cycles using lignin as feedstock (not reported in this work) was subjected to XRD analysis. Noticeably, the MoO_3-related peaks had decreased in intensity for the spent catalyst (see Fig. S3). From molybdenum-containing catalysts used for the oxidation of methanol in the temperature range of 300-400 °C, it is known that Mo can form volatile species with methanol and also with water [76–81]. Despite the presence of small oxygenates including MeOH and ~15 vol.% steam during reaction conditions, the analysis of the Mo content of the spent catalyst amounted to 6.7 wt%. As such, no loss of Mo could be concluded within this work, indicating a strong interaction with the support. The smaller and broader MoO_3-related peaks observed for the spent sample may indicate that MoO_3 on the fresh MoO_3/TiO_2 dispersed into smaller and better-distributed domains under the reaction conditions.

3.6 Energy recovery

It is of interest to benchmark the performance of the HDO catalysts against each other and against other acidic catalysts such as HZSM-5 zeolite, Al_2O_3, and HZSM-5/Al_2O_3 extrudates [14,62]. Fig. 6 shows the degree of deoxygenation (DOD) obtained in the collected bio-oil and their energy recovery with respect to bio-oil obtained without catalyst in N_2 atmosphere. When using acidic catalysts for vapor upgrading under N_2 atmosphere, the deoxygenation rapidly decreased towards higher B:C ratio while the energy recovery of the oil increased (Fig. 6). Interestingly, a ~5% higher energy recovery of the condensed oil phase was obtained when switching to 50 vol.% H_2 without using a catalyst. This is attributed to a slight hydrodeoxygenation achieved by the metal surfaces inside the pyrolysis system or metals in the char/ash with catalytic activity, which is consistent with a slight increase in reaction water due to HDO and a reduction

672 in the oil's oxygen content by 20%. While the overall yield of liquid-range organics was
673 comparable (Fig. 1), this led to a more favorable phase separation between organic and aqueous
674 phase with a decreased yield of (polar) organic compounds in the aqueous phase. The application
675 of atmospheric HDO achieved higher energy recoveries for a given level of deoxygenation
676 compared to the acidic catalysts (Fig. 6). While obtaining the same energy recovery as the non-
677 catalytic oil (N_2), almost 60% deoxygenation was achieved with Pt/TiO_2 at B:C ~4 and 50 vol.%
678 H_2. Note that at lower B:C (1.4) a lower oxygen content can be obtained albeit at lower energy
679 recovery due to increased losses to gas and coke (Fig. 1). Amongst the three HDO catalysts tested
680 at 50 vol.% H_2, the industrial Mo based catalyst achieved the lowest energy recoveries compared
681 at similar vapor deoxygenation, which correlated with higher gas and coke yields. At 50 vol.% H_2,
682 MoO_3/TiO_2 performed identical to Pt/TiO_2 in terms of deoxygenation and energy recovery of
683 condensed bio-oil: ~60% deoxygenation of oil was obtained at a similar energy recovery (101%)
684 of bio-oil fraction compared to the non-catalytic reference case without hydrogen addition. The
685 lower hydrogenation activity of Mo compared to Pt was seemingly compensated by the
686 significantly higher loading of Mo on TiO_2 (11 times higher than Pt) leading to roughly similar
687 activity of the two catalysts. An increase in H_2 partial pressure from 50 to 90 vol.% H_2 further
688 increased the deoxygenation and energy recovery of the bio-oils. At 90 vol.% H_2, energy recoveries
689 of bio-oil with respect to the fed biomass of 42 and 39% were obtained with bio-oil oxygen
690 contents of 10 and 8 wt.% (d.b.) using the Pt/TiO_2 and MoO_3/TiO_2 catalyst, respectively. With
691 operation to B:C of 7-8, the extent of deoxygenation decreased for both Pt/TiO_2 and MoO_3/TiO_2
692 catalyst while the oil yield increased (see Fig. 1). For Pt/TiO_2 this led to a slight increase in energy
693 recovery, while for MoO_3/TiO_2 the energy recovery decreased due to the lower heating value of

the oil (36.5 vs. 37.7 MJ/kg), thereby approaching the results obtained at lower H_2 concentration and B:C ~4.

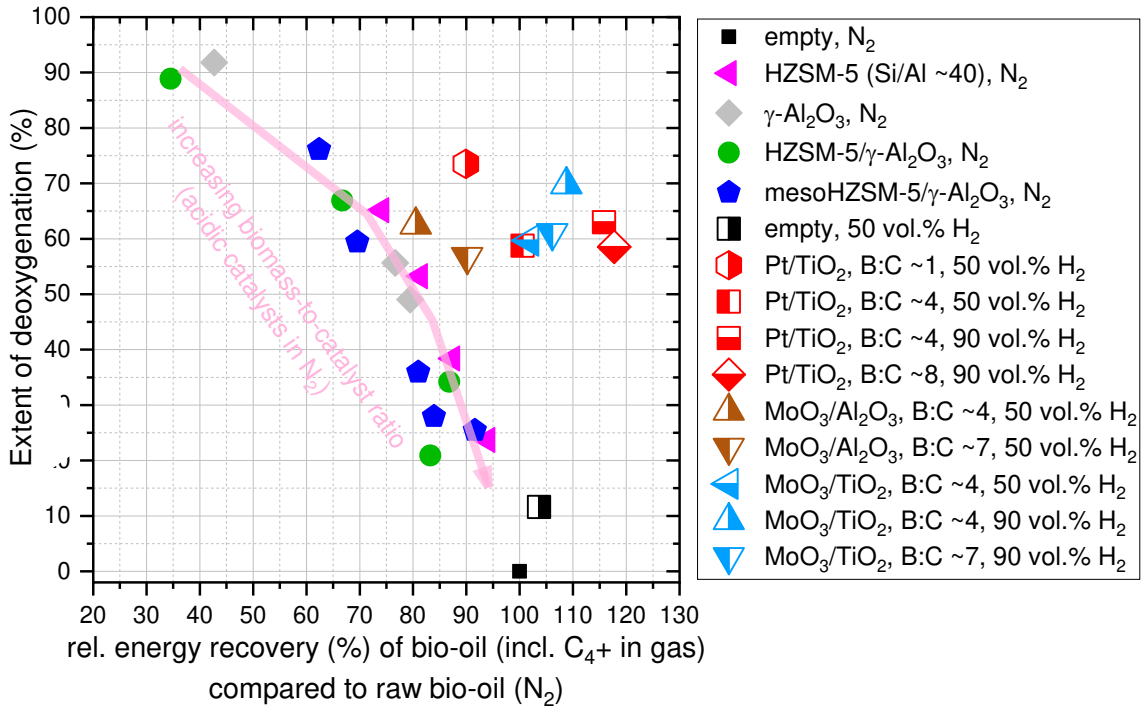

Fig. 6. Deoxygenation and energy recovery of bio-oil obtained with HDO catalysts at 400-450 °C (half-filled symbols) and acidic catalysts at 500 °C (filled symbols) relative to a non-catalytic bio-oil obtained under inert conditions (N_2) with 26 wt.% O (d.b.) and 36% energy recovery.

3.7 Catalyst cost estimation

In order to obtain a rough cost comparison of the two in-house prepared TiO_2-supported catalysts, the estimation tool CatCost [82], provided by the DOE/NREL/ALLIANCE, was used. The material cost of 10 wt.% MoO_3/TiO_2 catalyst was estimated to be ~4300 $/ton of catalyst, with zero value of the spent catalyst. The material cost of 0.5 wt.% Pt/TiO_2 catalyst was significantly higher (~118000 $/ton of catalyst), but the spent catalyst value was estimated to be ~92700 $/ton of catalyst. The Pt catalyst therefore has much higher investment costs, and even when taking the value of the spent catalyst into account, the Pt/TiO_2 catalyst would be almost 6 times more expensive compared to the 10 wt.% MoO_3/TiO_2 catalyst. This speaks for the latter catalyst, since it achieved similar performance to Pt/TiO_2, especially at higher H_2 partial pressure; however,

710 further optimization of the Pt loading of the Pt/TiO_2, and possibly Pt particle size [83,84], should
711 be carried out before a firm conclusion can be drawn.

712 4 CONCLUSION

713 Atmospheric hydro-deoxygenation (HDO) of wheat straw fast pyrolysis vapors was investigated
714 in a continuous flow setup using 100 g of 0.5 wt.% Pt/TiO_2, 10 wt.% MoO_3/TiO_2, or an industrial
715 MoO_3/Al_2O_3 catalyst. The HDO provided higher energy recoveries of bio-oils compared to acidic
716 catalysts such as γ-Al_2O_3 or HZSM-5 zeolite, which is attributed to carbon preserving HDO
717 reactions, H_2 incorporation, and a reduction in polarity of the compounds, thereby reducing losses
718 to the aqueous phase. At 50 vol.% H_2, the performance of the industrial Mo based catalyst was the
719 poorest, with the highest gas and coke yields. 10 wt.% MoO_3/TiO_2 performed identical to 0.5 wt.%
720 Pt/TiO_2 at 50 vol.% H_2 and obtained oil with ~11 wt.% O, 31 C% and 36% energy recovery. The
721 carbon and energy recovery could be further improved by increasing the hydrogen concentration
722 in the gas to ~90 vol.%, yielding oils with 8-10 wt.% O (dry basis) and 39-42 % energy recovery.
723 This further decreased the acidity (TAN) of the bio-oil to as low as 2 mg KOH/g when using
724 Pt/TiO_2 (non-catalytic = 66 mg KOH/g). Oils obtained from HDO using Pt/TiO_2 catalyst showed
725 a higher aliphatic content compared to the Mo based catalysts, which reduced the charring
726 tendency during heating of the bio-oil. Methoxyphenols that are present in non-treated bio-oil were
727 not detected in the upgraded bio-oils and thus were likely converted to aromatic hydrocarbons or
728 partially deoxygenated into phenols.

729 For the deoxygenation of biomass fast pyrolysis vapors, it is critical to balance the
730 deoxygenation severity with the carbon losses during deoxygenation. The application of
731 atmospheric pressure catalytic HDO reduced the losses of carbon to the aqueous phase and coke
732 and increased the carbon recovery of bio-oil with improved fuel properties, which may be further

processed in conventional refineries or directly applied as a renewable fuel, e.g. for ship engines. The presented data may facilitate future techno-economic assessment for the production of transportation fuels from agricultural residues.

ASSOCIATED CONTENT

Supporting Information: Scheme of bench-scale fast pyrolysis unit; Temperature of catalyst during reaction; Isotherms and pore size distribution from N_2 physisorption; NH_3-TPD acidity characterization; Pyridine FT-IR characterization; pre and post-reaction TEM images and particle size distribution; concentration of light hydrocarbons during reaction over Pt/TiO_2; thermo-gravimetric analysis of bio-oils; GC × GC plots; ^{13}C NMR and 2D NMR spectra of bio-oils;

AUTHOR INFORMATION

Corresponding Author:

* aj@kt.dtu.dk (Anker Degn Jensen)

Author Contributions

The manuscript was written through contributions of all authors. All authors have given approval to the final version of the manuscript.

CONFLICTS OF INTEREST

There are no conflicts to declare.

ACKNOWLEDGMENT

Funding by the Danish Energy Technology Development and Demonstration Program (EUDP project number 12454) is gratefully acknowledged. Alireza Saraeian and Brent H. Shanks would

like to acknowledge funding from the Iowa Energy Center, Iowa Economic Development Authority and its utility partners under the grant number 17-IEC-002.

ABBREVIATIONS

daf, dry and ash-free; d.b., dry basis; DOD, degree of deoxygenation; FID, flame ionization detection; GC, gas chromatography; HDO, hydrodeoxygenation, MS, mass spectrometry; TEM, transmission electron microscopy; TGA, thermogravimetric analysis; TPD, temperature-programmed desorption;

REFERENCES

[1] A.J. Toft, A comparison of integrated biomass to electricity systems, The University of Aston in Birmingham, 1996.

[2] D. Mourant, C. Lievens, R. Gunawan, Y. Wang, X. Hu, L. Wu, S.S.A. Syed-Hassan, C.-Z. Li, Effects of temperature on the yields and properties of bio-oil from the fast pyrolysis of mallee bark, Fuel. 108 (2013) 400–408. doi:10.1016/J.FUEL.2012.12.018.

[3] N. Ibrahim, Bio-oil from Flash Pyrolysis of Agricultural Residues, DTU Chemical Engineering, 2012. https://orbit.dtu.dk/en/publications/bio-oil-from-flash-pyrolysis-of-agricultural-residues (accessed November 28, 2019).

[4] D.S. Scott, J. Piskorz, The Continuous Flash Pyrolysis of Biomass, Can. J. Chem. Eng. 62 (1984) 404.

[5] N. Bech, M.B. Larsen, P.A. Jensen, K. Dam-Johansen, Modelling solid-convective flash pyrolysis of straw and wood in the Pyrolysis Centrifuge Reactor, Biomass and Bioenergy. 33 (2009) 999–1011. doi:10.1016/j.biombioe.2009.03.009.

[6] H. Hernando, S. Jiménez-Sánchez, J. Fermoso, P. Pizarro, J.M. Coronado, D.P. Serrano, Assessing biomass catalytic pyrolysis in terms of deoxygenation pathways and energy yields for the efficient production of advanced biofuels, Catal. Sci. Technol. 6 (2016) 2829–2843. doi:10.1039/c6cy00522e.

[7] H.L. Chum, R.P. Overend, Biomass and renewable fuels, Fuel Process. Technol. 71 (2001) 187–195. doi:10.1016/S0378-3820(01)00146-1.

[8] M. Shemfe, S. Gu, B. Fidalgo, Techno-economic analysis of biofuel production via bio-oil zeolite upgrading: An evaluation of two catalyst regeneration systems, Biomass and Bioenergy. 98 (2017) 182–193. doi:10.1016/j.biombioe.2017.01.020.

[9] L. Faba, E. Díaz, S. Ordóñez, Recent developments on the catalytic technologies for the transformation of biomass into biofuels: A patent survey, Renew. Sustain. Energy Rev. 51 (2015) 273–287. doi:10.1016/j.rser.2015.06.020.

[10] M.S. Talmadge, R.M. Baldwin, M.J. Biddy, R.L. McCormick, G.T. Beckham, G.A. Ferguson, S. Czernik, K. Magrini, T.D. Foust, P.D. Metelski, C. Hetrick, M.R. Nimlos, A perspective on oxygenated species in the refinery integration of pyrolysis oil, Green Chem. 16 (2014) 407–453. doi:10.1039/C3GC41951G.

[11] A. V. Bridgwater, Review of fast pyrolysis of biomass and product upgrading, Biomass and Bioenergy. 38 (2012) 68–94. doi:10.1016/j.biombioe.2011.01.048.

[12] R. French, S. Czernik, Catalytic pyrolysis of biomass for biofuels production, Fuel Process. Technol. 91 (2010) 25–32. doi:10.1016/j.fuproc.2009.08.011.

[13] A. Eschenbacher, P.A. Jensen, U.B. Henriksen, J. Ahrenfeldt, C. Li, J.Ø. Duus, U.V. Mentzel, A.D. Jensen, Impact of ZSM-5 deactivation on bio-oil quality during upgrading of straw derived pyrolysis vapors, Energy & Fuels. 33 (2019) 397–412. doi:10.1021/acs.energyfuels.8b03691.

[14] A. Eschenbacher, P.A. Jensen, U.B. Henriksen, J. Ahrenfeldt, C. Li, J.Ø. Duus, U.V. Mentzel, A.D. Jensen, Deoxygenation of wheat straw fast pyrolysis vapors using HZSM-5, Al2O3 , HZSM-5/Al2O3 extrudates, and desilicated HZSM-5/Al2O3 extrudates, Energy & Fuels. (2019) acs.energyfuels.9b00906. doi:10.1021/acs.energyfuels.9b00906.

[15] A. Oasmaa, D.C. Elliott, J. Korhonen, Acidity of biomass fast pyrolysis bio-oils, Energy and Fuels. 24 (2010) 6548–6554. doi:10.1021/ef100935r.

[16] S. Bezergianni, A. Dimitriadis, O. Kikhtyanin, D. Kubička, Refinery co-processing of renewable feeds, Prog. Energy Combust. Sci. 68 (2018) 29–64. doi:10.1016/j.pecs.2018.04.002.

[17] C. Wang, M. Li, Y. Fang, Coprocessing of Catalytic-Pyrolysis-Derived Bio-Oil with VGO in a Pilot-Scale FCC Riser, Ind. Eng. Chem. Res. 55 (2016) 3525–3534. doi:10.1021/acs.iecr.5b03008.

[18] A. Oasmaa, S. Czernik, Fuel oil quality of biomass pyrolysis oil - State of the art for the end users, Energy & Fuels. 13 (1999) 914–921. doi:10.1021/ef980272b.

[19] S. Czernik, A. V. Bridgwater, Overview of applications of biomass fast pyrolysis oil, Energy & Fuels. 18 (2004) 590–598. doi:10.1021/ef034067u.

[20] A. Saraeian, M.W. Nolte, B.H. Shanks, Deoxygenation of biomass pyrolysis vapors: Improving clarity on the fate of carbon, Renew. Sustain. Energy Rev. 104 (2019) 262–280. doi:10.1016/j.rser.2019.01.037.

[21] R.H. Venderbosch, A critical view on catalytic pyrolysis of biomass, ChemSusChem. 8 (2015) 1306–1316. doi:10.1002/cssc.201500115.

[22] J. Jae, G.A. Tompsett, A.J. Foster, K.D. Hammond, S.M. Auerbach, R.F. Lobo, G.W. Huber, Investigation into the shape selectivity of zeolite catalysts for biomass conversion, J. Catal. 279 (2011) 257–268.

doi:10.1016/j.jcat.2011.01.019.
[23] T.R. Carlson, G.A. Tompsett, W.C. Conner, G.W. Huber, Aromatic production from catalytic fast pyrolysis of biomass-derived feedstocks, Top. Catal. 52 (2009) 241–252. doi:10.1007/s11244-008-9160-6.
[24] P.A. Horne, P.T. Williams, The effect of zeolite ZSM-5 catalyst deactivation during the upgrading of biomass-derived pyrolysis vapours, J. Anal. Appl. Pyrolysis. 34 (1995) 65–85. doi:10.1016/0165-2370(94)00875-2.
[25] S. Wan, T. Pham, S. Zhang, L. Lobban, D. Resasco, R. Mallinson, Direct catalytic upgrading of biomass pyrolysis vapors by a dual function Ru/TiO $_2$ catalyst, AIChE J. 59 (2013) 2275–2285. doi:10.1002/aic.14038.
[26] R. Kumar, N. Enjamuri, S. Shah, A.S. Al-Fatesh, J.J. Bravo-Suárez, B. Chowdhury, Ketonization of oxygenated hydrocarbons on metal oxide based catalysts, Catal. Today. (2017). doi:10.1016/j.cattod.2017.09.044.
[27] T.N. Pham, T. Sooknoi, S.P. Crossley, D. Resasco, Ketonization of carboxylic acids: Mechanism, catalysts, and implications for biomass concersion, Am. Chem. Soc. Catal. 3 (2013) 2456–2473.
[28] O. Nagashima, S. Sato, R. Takahashi, T. Sodesawa, Ketonization of carboxylic acids over CeO 2-based composite oxides, J. Mol. Catal. A Chem. 227 (2005) 231–239. doi:10.1016/j.molcata.2004.10.042.
[29] O.D. Mante, J. a. Rodriguez, S.D. Senanayake, S.P. Babu, Catalytic conversion of biomass pyrolysis vapors into hydrocarbon fuel precursors, Green Chem. 17 (2015) 2362–2368. doi:10.1039/C4GC02238F.
[30] Q. Lu, Y. Zhang, Z. Tang, W.Z. Li, X.F. Zhu, Catalytic upgrading of biomass fast pyrolysis vapors with titania and zirconia/titania based catalysts, Fuel. 89 (2010) 2096–2103. doi:10.1016/j.fuel.2010.02.030.
[31] Q. Lu, Z.B. Zhang, X.Q. Wang, C.Q. Dong, Y.Q. Liu, Catalytic upgrading of biomass fast pyrolysis vapors using ordered mesoporous ZrO2, TiO2 and SiO2, Energy Procedia. 61 (2014) 1937–1941. doi:10.1016/j.egypro.2014.12.247.
[32] P. Kaewpengkrow, D. Atong, V. Sricharoenchaikul, Catalytic upgrading of pyrolysis vapors from Jatropha wastes using alumina, zirconia and titania based catalysts, Bioresour. Technol. 163 (2014) 262–269. doi:10.1016/j.biortech.2014.04.035.
[33] K.S. Kim, M.A. Barteau, Structure and composition requirements for deoxygenation, dehydration, and ketonization reactions of carboxylic acids on TiO2(001) single-crystal surfaces, J. Catal. 125 (1990) 353–375. doi:10.1016/0021-9517(90)90309-8.
[34] R. Pestman, R.M. Koster, A. van Duijne, J.A.Z. Pieterse, V. Ponec, Reactions of Carboxylic Acids on Oxides, J. Catal. 168 (1997) 265–272. doi:10.1006/jcat.1997.1624.
[35] O.D. Mante, J.A. Rodriguez, S.P. Babu, Selective defunctionalization by TiO2 of monomeric phenolics from lignin pyrolysis into simple phenols, Bioresour. Technol. 148 (2013) 508–516. doi:10.1016/j.biortech.2013.09.003.
[36] M.B. Griffin, G.A. Ferguson, D.A. Ruddy, M.J. Biddy, G.T. Beckham, J.A. Schaidle, Role of the Support and Reaction Conditions on the Vapor-Phase Deoxygenation of m-Cresol over Pt/C and Pt/TiO2 Catalysts, ACS Catal. 6 (2016) 2715–2727. doi:10.1021/acscatal.5b02868.
[37] S.M. Schimming, O.D. LaMont, M. König, A.K. Rogers, A.D. D'Amico, M.M. Yung, C. Sievers, Hydrodeoxygenation of Guaiacol over Ceria-Zirconia Catalysts, ChemSusChem. 8 (2015) 2073–2083. doi:10.1002/cssc.201500317.
[38] P.M. de Souza, R.C. Rabelo-Neto, L.E.P. Borges, G. Jacobs, B.H. Davis, U.M. Graham, D.E. Resasco, F.B. Noronha, Effect of Zirconia Morphology on Hydrodeoxygenation of Phenol over Pd/ZrO $_2$, ACS Catal. 5 (2015) 7385–7398. doi:10.1021/acscatal.5b01501.
[39] S. Boonyasuwat, T. Omotoso, D.E. Resasco, S.P. Crossley, Conversion of guaiacol over supported Ru catalysts, Catal. Letters. 143 (2013) 783–791. doi:10.1007/s10562-013-1033-3.
[40] M.B. Griffin, G.A. Ferguson, D.A. Ruddy, M.J. Biddy, G.T. Beckham, J.A. Schaidle, Role of the Support and Reaction Conditions on the Vapor-Phase Deoxygenation of *m* -Cresol over Pt/C and Pt/TiO $_2$ Catalysts, ACS Catal. 6 (2016) 2715–2727. doi:10.1021/acscatal.5b02868.
[41] M.B. Griffin, K. Iisa, H. Wang, A. Dutta, K.A. Orton, R.J. French, D.M. Santosa, A.N. Wilson, E.D. Christensen, C. Nash, F.G. Baddour, K. Van Allsburg, D.A. Ruddy, C. Mukarakate, J.A. Schaidle, Driving towards cost-competitive biofuels through catalytic fast pyrolysis by rethinking catalyst selection and reactor configuration, Energy Environ. Sci. Accepted w (2018). doi:10.1039/C8EE01872C.
[42] T. Prasomsri, T. Nimmanwudipong, Y. Román-Leshkov, Effective hydrodeoxygenation of biomass-derived oxygenates into unsaturated hydrocarbons by MoO3 using low H2 pressures, Energy Environ. Sci. 6 (2013) 1732. doi:10.1039/c3ee24360e.
[43] M. Shetty, K. Murugappan, T. Prasomsri, W.H. Green, Y. Román-Leshkov, Reactivity and stability investigation of supported molybdenum oxide catalysts for the hydrodeoxygenation (HDO) of m-cresol, J. Catal. 331 (2015) 86–97. doi:10.1016/j.jcat.2015.07.034.

[44] T. Prasomsri, M. Shetty, K. Murugappan, Y. Román-Leshkov, Insights into the catalytic activity and surface modification of MoO_3 during the hydrodeoxygenation of lignin-derived model compounds into aromatic hydrocarbons under low hydrogen pressures, Energy Environ. Sci. 7 (2014) 2660–2669. doi:10.1039/C4EE00890A.
[45] M.W. Nolte, J. Zhang, B.H. Shanks, Ex situ hydrodeoxygenation in biomass pyrolysis using molybdenum oxide and low pressure hydrogen, Green Chem. 18 (2015) 134–138. doi:10.1039/c5gc01614b.
[46] G. Zhou, P.A. Jensen, D.M. Le, N.O. Knudsen, A.D. Jensen, Atmospheric Hydrodeoxygenation of Biomass Fast Pyrolysis Vapor by MoO3, ACS Sustain. Chem. Eng. 4 (2016) 5432–5440. doi:10.1021/acssuschemeng.6b00757.
[47] K. Murugappan, C. Mukarakate, S. Budhi, M. Shetty, M.R. Nimlos, Y. Román-Leshkov, Supported molybdenum oxides as effective catalysts for the catalytic fast pyrolysis of lignocellulosic biomass, Green Chem. 18 (2016) 5548–5557. doi:10.1039/C6GC01189F.
[48] K. Wang, D.C. Dayton, J.E. Peters, O.D. Mante, Reactive catalytic fast pyrolysis of biomass to produce high-quality bio-crude, Green Chem. 19 (2017) 3243–3251. doi:10.1039/c7gc01088e.
[49] D.P. Gamliel, G.M. Bollas, J.A. Valla, Two-stage catalytic fast hydropyrolysis of biomass for the production of drop-in biofuel, Fuel. 216 (2018) 160–170. doi:10.1016/j.fuel.2017.12.017.
[50] D.P. Gamliel, G.M. Bollas, J.A. Valla, Bifunctional Ni-ZSM-5 Catalysts for the Pyrolysis and Hydropyrolysis of Biomass, Energy Technol. 5 (2017) 172–182. doi:10.1002/ente.201600136.
[51] A. Galadima, O. Muraza, In situ fast pyrolysis of biomass with zeolite catalysts for bioaromatics/gasoline production: A review, Energy Convers. Manag. 105 (2015) 338–354. doi:10.1016/j.enconman.2015.07.078.
[52] S. Wan, Y. Wang, A review on ex situ catalytic fast pyrolysis of biomass, Front. Chem. Sci. Eng. 8 (2014) 280–294. doi:10.1007/s11705-014-1436-8.
[53] C. Liu, H. Wang, A.M. Karim, J. Sun, Y. Wang, Catalytic fast pyrolysis of lignocellulosic biomass, Chem. Soc. Rev. 43 (2014) 7594–7623. doi:10.1039/C3CS60414D.
[54] T.J. Mazanec, J.P. Whiting, F. Pesa, R. Song, Y.-T. Cheng, R. Song, Regeneration of catalytic fast pyrolysis, US 2014/0303414 A1, 2017.
[55] J. Shi, C. Sorensen, T. Mazanec, R. Song, S. Goud, S. Han, Y.-T. Cheng, V.L. Frank, J.W.F. Igoe, M. Schneidkraut, Improved catalytic fast pyrolysis process with impurity removal, WO2017003790A1, 2015.
[56] V. Paasikallio, C. Lindfors, E. Kuoppala, Y. Solantausta, A. Oasmaa, J. Lehto, J. Lehtonen, Product quality and catalyst deactivation in a four day catalytic fast pyrolysis production run, Green Chem. 16 (2014) 3549–3559. doi:10.1039/c4gc00571f.
[57] K.G. Kalogiannis, S.D. Stefanidis, A.A. Lappas, Catalyst deactivation, ash accumulation and bio-oil deoxygenation during ex situ catalytic fast pyrolysis of biomass in a cascade thermal-catalytic reactor system, Fuel Process. Technol. 186 (2019) 99–109. doi:10.1016/j.fuproc.2018.12.008.
[58] A. Dutta, J.A. Schaidle, D. Humbird, F.G. Baddour, A. Sahir, Conceptual Process Design and Techno-Economic Assessment of Ex Situ Catalytic Fast Pyrolysis of Biomass: A Fixed Bed Reactor Implementation Scenario for Future Feasibility, Top. Catal. 59 (2016) 2–18. doi:10.1007/s11244-015-0500-z.
[59] J.T. Miller, M. Schreier, A.J. Kropf, J.R. Regalbuto, A fundamental study of platinum tetraammine impregnation of silica: 2. The effect of method of preparation, loading, and calcination temperature on (reduced) particle size, J. Catal. 225 (2004) 203–212. doi:10.1016/j.jcat.2004.04.007.
[60] M. Schreier, J.R. Regalbuto, A fundamental study of Pt tetraammine impregnation of silica: 1. The electrostatic nature of platinum adsorption, J. Catal. 225 (2004) 190–202. doi:10.1016/j.jcat.2004.03.034.
[61] A. Eschenbacher, F. Goodarzi, A. Saraeian, S. Kegnæs, B.H. Shanks, A.D. Jensen, Performance of Mesoporous HZSM-5 and Silicalite-1 Coated Mesoporous HZSM-5 Catalysts for Deoxygenation of Straw Fast Pyrolysis Vapors, J. Anal. Appl. Pyrolysis. (2019) 104712. doi:10.1016/J.JAAP.2019.104712.
[62] A. Eschenbacher, P.A. Jensen, U.B. Henriksen, J. Ahrenfeldt, S. Ndoni, C. Li, J.Ø. Duus, U.V. Mentzel, A.D. Jensen, Catalytic deoxygenation of vapors obtained from ablative fast pyrolysis of wheat straw using mesoporous HZSM-5, Fuel Process. Technol. 194 (2019) 106119. doi:10.1016/J.FUPROC.2019.106119.
[63] S.A. Channiwala, P.P. Parikh, A unified correlation for estimating HHV of solid, liquid and gaseous fuels, Fuel. 81 (2002) 1051–1063. doi:10.1016/S0016-2361(01)00131-4.
[64] K. Schofield, The enigmatic mechanism of the flame ionization detector: Its overlooked implications for fossil fuel combustion modeling, Prog. Energy Combust. Sci. 34 (2008) 330–350. doi:10.1016/j.pecs.2007.08.001.
[65] M. Von Holle, J.R. Carpenter, D.C. Dayton, Reactive catalytic fast pyrolysis process and system, US 2019/0211268 Al, 2019. doi:10.1111/2047-8852.12112.
[66] D.C. Dayton, T. Member, A. Daniels, M. Company, Catalytic Deoxygenation of Biomass Pyrolysis Vapors to Improve Bio-oil Stability, n.d.

[67] H. Ben, A.J. Ragauskas, Heteronuclear single-quantum correlation-nuclear magnetic resonance (HSQC-NMR) fingerprint analysis of pyrolysis oils, Energy and Fuels. 25 (2011) 5791–5801. doi:10.1021/ef201376w.
[68] R.M. Happs, K. Iisa, J.R.F. Iii, Quantitative 13C NMR characterization of fast pyrolysis oils, RSC Adv. 6 (2016) 102665–102670. doi:10.1039/C6RA24044E.
[69] M.B. Griffin, K. Iisa, H. Wang, A. Dutta, K.A. Orton, R.J. French, D.M. Santosa, N. Wilson, E. Christensen, C. Nash, K.M. Van Allsburg, F.G. Baddour, D.A. Ruddy, E.C.D. Tan, H. Cai, C. Mukarakate, J.A. Schaidle, Driving towards cost-competitive biofuels through catalytic fast pyrolysis by rethinking catalyst selection and reactor configuration, Energy Environ. Sci. 11 (2018) 2904–2918. doi:10.1039/c8ee01872c.
[70] T.T. Pham, L.L. Lobban, D.E. Resasco, R.G. Mallinson, Hydrogenation and Hydrodeoxygenation of 2-methyl-2-pentenal on supported metal catalysts, J. Catal. 266 (2009) 9–14. doi:10.1016/j.jcat.2009.05.009.
[71] J.G. Speight, Corrosion by High Acid Crude Oil, in: High Acid Crudes, Elsevier, 2014: pp. 57–75. doi:10.1016/B978-0-12-800630-6.00003-4.
[72] N.Y. Chen, D.E. Walsh, L.R. Koenig, Fluidized Bed Upgrading of Wood Pyrolysis Liquids and Related Compounds., ACS Div. Fuel Chem. Prepr. 32 (1987) 264–275. doi:10.1021/bk-1988-0376.ch024.
[73] S.D. Gray, K.J. Weller, M.A. Bruck, P.M. Briggs, D.E. Wigley, Carbon—Nitrogen Bond Cleavage in an η2(N, C)-Pyridine Complex Induced by Intramolecular Metal-to-Ligand Alkyl Migration: Models for Hydrodenitrogenation Catalysis, J. Am. Chem. Soc. 117 (1995) 10678–10693. doi:10.1021/ja00148a010.
[74] T.N. Pham, T. Sooknoi, S.P. Crossley, D.E. Resasco, Ketonization of Carboxylic Acids: Mechanisms, Catalysts, and Implications for Biomass Conversion, ACS Catal. 3 (2013) 2456–2473. doi:10.1021/cs400501h.
[75] T.M.H. Dabros, M.Z. Stummann, M. Høj, P.A. Jensen, J.D. Grunwaldt, J. Gabrielsen, P.M. Mortensen, A.D. Jensen, Transportation fuels from biomass fast pyrolysis, catalytic hydrodeoxygenation, and catalytic fast hydropyrolysis, Prog. Energy Combust. Sci. 68 (2018) 268–309. doi:10.1016/j.pecs.2018.05.002.
[76] K.V. Raun, L.F. Lundegaard, J. Chevallier, P. Beato, C.C. Appel, K. Nielsen, M. Thorhauge, A.D. Jensen, M. Høj, Deactivation behavior of an iron-molybdate catalyst during selective oxidation of methanol to formaldehyde, Catal. Sci. Technol. 8 (2018) 4626–4637. doi:10.1039/c8cy01109e.
[77] K.I. Ivanov, D.Y. Dimitrov, Deactivation of an industrial iron-molybdate catalyst for methanol oxidation, in: Catal. Today, 2010: pp. 250–255. doi:10.1016/j.cattod.2010.03.051.
[78] K.V. Raun, M. Thorhauge, M. Høj, A.D. Jensen, Modeling of molybdenum transport and pressure drop increase in fixed bed reactors used for selective oxidation of methanol to formaldehyde using iron molybdate catalysts, Chem. Eng. Sci. 202 (2019) 347–356. doi:10.1016/j.ces.2019.03.020.
[79] J. Thrane, L.F. Lundegaard, P. Beato, U.V. Mentzel, M. Thorhauge, A.D. Jensen, M. Høj, Alkali Earth Metal Molybdates as Catalysts for the Selective Oxidation of Methanol to Formaldehyde—Selectivity, Activity, and Stability, Catalysts. 10 (2020) 82. doi:10.3390/catal10010082.
[80] A.P.V. Soares, M.F. Portela, A. Kiennemann, L. Hilaire, Mechanism of deactivation of iron-molybdate catalysts prepared by coprecipitation and sol - gel techniques in methanol to formaldehyde oxidation, Chem. Eng. Sci. 58 (2003) 1315–1322. doi:10.1016/S0009-2509(02)00573-0.
[81] K. Routray, W. Zhou, C.J. Kiely, W. Grünert, I.E. Wachs, Origin of the synergistic interaction between MoO3 and iron molybdate for the selective oxidation of methanol to formaldehyde, J. Catal. 275 (2010) 84–98. doi:10.1016/j.jcat.2010.07.023.
[82] CatCost, (n.d.). https://catcost.chemcatbio.org/ (accessed November 13, 2019).
[83] P.M. Mortensen, J.D. Grunwaldt, P.A. Jensen, A.D. Jensen, Influence on nickel particle size on the hydrodeoxygenation of phenol over Ni/SiO2, Catal. Today. 259 (2016) 277–284. doi:10.1016/j.cattod.2015.08.022.
[84] C. Newman, X. Zhou, B. Goundie, I.T. Ghampson, R.A. Pollock, Z. Ross, M.C. Wheeler, R.W. Meulenberg, R.N. Austin, B.G. Frederick, Effects of support identity and metal dispersion in supported ruthenium hydrodeoxygenation catalysts, Appl. Catal. A Gen. 477 (2014) 64–74. doi:10.1016/j.apcata.2014.02.030.